To the Graduate Council:

I am submitting herewith a thesis written by Jessee Americus Scarborough entitled "Estimation and Impact of Surface Subsidence in a Karst Terrain." I have examined the final copy of this thesis for form and content and recommend that it be accepted in partial fulfillment of the requirements for the degree of Master of Science, with a major in Civil Engineering.

William F. Kane

William F. Kane, Major Professor

We have read this thesis
and recommend its acceptance:

Eric C. Drumm

Richard M. Bennett

Richard H. Ketchum

Accepted for the Council:

Lou Pinkel

Vice Provost
and Dean of The Graduate School

STATEMENT OF PERMISSION TO USE

In presenting this thesis in partial fulfillment of the requirements for a Master's degree at The University of Tennessee, Knoxville, I agree that the Library shall make it available to borrowers under rules of the library. Brief quotations from this thesis are allowable without special permission, provided that accurate acknowledgement of the source is made.

Requests for permission for extensive quotation from or reproduction of this thesis in whole or in parts may be granted by the copyright holder.

Signature James A. Sanchez

Date 30 November 1989

ESTIMATION AND IMPACT OF SURFACE SUBSIDENCE IN A KARST TERRAIN

A Thesis

Presented for the

Master of Science

Degree

The University of Tennessee, Knoxville

Jessee Americus Scarborough

December 1989

Copyright © Jessee Americus Scarborough, 1990
All rights reserved

ACKNOWLEDGMENTS

First, I would like to acknowledge the patience and direction provided by my major professor, Dr. William F. Kane, and my other committee members, Dr. Eric C. Drumm and Dr. Richard M. Bennett, all of the University of Tennessee, Knoxville, Department of Civil Engineering. Also, Mr. Richard H. Ketelle, of Martin Marietta Energy Systems, Inc., for providing the opportunity and the sinkholes, and Mr. S. Colin Kinton whose assistance in the field was invaluable. Mr. J. Ben-Hassine's efforts to develop and apply nonlinear, finite element analysis deserve recognition.

Next, my parents who have kindly put me up and put up with me for the past year and a half. None of this would have been possible but for their love and patience.

And finally, to my friends and associates, I thank you for your support, with emphasis to Mr. and Mrs. Matthew S. Borgers and family.

ABSTRACT

The lateral and vertical extent of surface subsidence can contribute to the failure of surface structures. One method of empirical subsidence prediction which may have application in karst terrain is the use of profile functions. Application of this method involves fitting a mathematical function to a significant number of actual subsidence basin profiles. The resulting empirical constants describe the shape of the basin.

Ten dolines and one collapse on Chestnut Ridge, near the southeast corner of the Department of Energy's Oak Ridge, Tennessee Reservation, were surveyed. Two profile functions; the hyperbolic tangent function and the negative exponential function were fit to the field data. The negative exponential function is recommended. It provided a better fit to thirty-four of thirty-nine profiles.

The lateral extent of sinkhole subsidence is linearly related to the depth of overburden, while the magnitude of vertical displacement cannot be predicted from field data. Subsidence prediction requires an adequate assumption of subsurface geometry and behavior. Numerical analysis using the finite element method provided a valuable tool to identify significant relationships. Observed values of subsidence appear much greater than that required to cause severe damage to surface structures.

TABLE OF CONTENTS

SECTION	PAGE
ACKNOWLEDGMENTS	iii
ABSTRACT	iv
LIST OF TABLES	vii
LIST OF FIGURES	viii
LIST OF SYMBOLS	x
CHAPTER 1 INTRODUCTION	1
1.1 Purpose of the Study	1
1.2 Statement of the Problem	1
1.3 Note on Units	3
CHAPTER 2 LITERATURE REVIEW	4
2.1 Karst	4
2.2 Profile Functions	5
2.2.1 The Hyperbolic Tangent Function	8
2.2.2 The Negative Exponential Function	11
2.2.3 Slope and Curvature of Profile Functions	13
2.3 Magnitude and Extent of Subsidence	15
2.3.1 Angle of Draw	16
2.4 Structural Damage Associated with Subsidence	19
2.4.1 Sanitary Landfill Liner Systems	21
2.4.2 Damage Criteria for Buildings	23
CHAPTER 3 METHODOLOGY	26
3.1 Site Description	26
3.1.1 Geology	26
3.1.2 Soil Properties	29
3.2 Field Methods	34
3.2.1 Profile Selection	34
3.2.2 Survey Equipment	36
3.2.3 Survey Methods	36
3.3 Data Reduction	37
3.3.1 Plan and Profile	39
3.3.2 Determination of Empirical Parameters	40
CHAPTER 4 RESULTS	43
4.1 Profile Functions and Profiles	43

SECTION PAGE

4.1.1 Subsidence Prediction from Field Profiles 45
4.2 Idealization of Subsurface Geometry 47
4.3 Site Subsidence Prediction 54
4.4 Induced Ground Movements 54

CHAPTER 5 CONCLUSIONS 58

5.1 Conclusions 58
5.2 Recommendations for Future Work 59

REFERENCES 60

APPENDIXES 64

APPENDIX A 65

APPENDIX B 76

B.1 Field Profiles and the Exponential Function . 76
B.2 Field Profiles and the Hyperbolic Function . 77
B.3 Numerical Profiles, Geometric Parameters . . 78
B.4 Numerical Profiles, Exponential Function . . 79
B.5 Numerical Profiles, Hyperbolic Function . . . 79

VITA 81

LIST OF TABLES

TABLE		PAGE
2.1	Profile functions	9
2.2	Damage criteria for buildings	24
4.1	Critical values for structural damage from sinkhole subsidence at East Chestnut Ridge. . . .	56
4.2	Required soil cavity radius for values of critical maximum subsidence	56

LIST OF FIGURES

FIGURE		PAGE
1.1	Idealized deformation of a sanitary landfill liner due to subsidence	2
2.1	Formation of a cover-collapse sinkhole, and secondary slope failure	6
2.2	Surface expression of sinkholes due to the deformation of a subsurface void	7
2.3	Idealized profile and definition of terms for the hyperbolic function.	10
2.4	Idealized profile and definition of terms for the exponential function.	12
2.5	Plot of slope and curvature versus horizontal position.	14
2.6	Definition of the angle of draw in terms of the depth of overburden and basin half-width	18
2.7	Ground movements and induced forces	20
2.8	Idealized behavior of a liner system in the tension zone around a subsidence event	22
3.1	Location of the site	27
3.2	Variation of the percent passing a #200 sieve with elevation above bedrock	30
3.3	USC classification of site soils.	32
3.4	Casagrande's plasticity chart for site soils	32
3.5	Variation of liquidity index (LI) with elevation above bedrock	33
3.6	Location of sinkholes on the East Chestnut Ridge site	35
3.7	Survey grid, location, and orientation of the four profiles	38
3.8	Normalized field data and best fit of the exponential function	41

FIGURE PAGE

3.9 Normalized field data and best fit of the hyperbolic function 42

4.1 Comparison of empirical parameters, C and α, from field profiles 44

4.2 Comparison of empirical parameters, C and β, from field profiles 44

4.3 Location of the inflection point relative to basin half-width from the field data 46

4.4 Soil-cavity idealization 49

4.5 Exponential relationship between cavity radius and maximum subsidence from the numerical analysis . . 50

4.6 Angle of draw from the numerical analysis 50

4.7 Location of the inflection point relative to basin half-width from the numerical analysis 52

LIST OF SYMBOLS

Empirical Parameters

α = one of two empirical parameters in the negative exponential function
β = one of two empirical parameters in the negative exponential function
C = empirical parameter in the hyperbolic tangent function

Parameters of the Subsidence Basin

S_0 = maximum vertical subsidence
L = half-width of the subsidence basin
B = horizontal location of the inflection point
x or X = abscissa of any point on the profile
Z = ratio of X/L
S(x) = vertical displacement
i(x) = slope
k(x) = curvature
$d_h(x)$ = horizontal displacement
$\epsilon_h(x)$ = horizontal strain

Geometric Parameters in the Subsurface

δ = angle of draw
H = depth of overburden
r = radius of a soil cavity

Material and Index Properties

ϕ = angle of internal friction
c = cohesion
LL = liquid limit
PI = plasticity index
LI = liquidity index

Other Parameters

K = a generic constant
R^2 = square of the correlation coefficient

CHAPTER 1 INTRODUCTION

1.1 Purpose of the Study

Subsidence is the vertical and horizontal movement of the ground surface due to the deformation of subterranean void(s). It can be attributed specifically to causes such as extraction of coal, excessive pumping of ground water, consolidation of loose soils, and the formation of sinkholes.

Sinkholes, or dolines, are a characteristic geomorphic landform in karst terrain. The lateral and vertical extent of sinkhole subsidence or collapse can contribute to the failure of surface structures, such as sanitary landfill liners and leachate collection systems. Figure 1.1 shows a generalization of such a failure. The seemingly random nature of karst makes site characterization in these regions extremely difficult. The failure of a landfill liner is exacerbated by the geohydrological characteristics of karst. Potential consequences can be mitigated by the consideration of subsidence during the design of a liner system.

1.2 Statement of the Problem

The design of an adequate structure requires knowledge of the forces which act to disturb stability. The deformation of a landfill liner due to surface subsidence is an example of earth-structure interaction. Whitman and

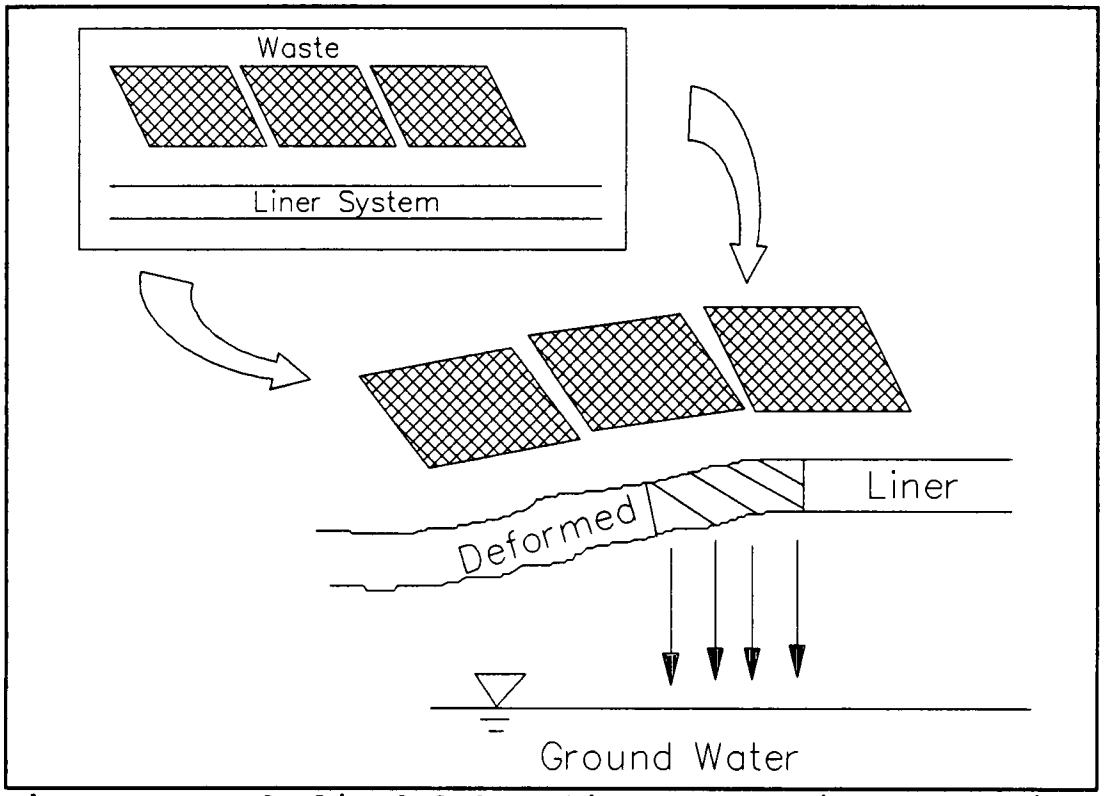


Figure 1.1 Idealized deformation of a sanitary landfill liner due to subsidence

Bielak (1980) have defined earth-structure interaction as:

> If the motion at any point on the soil-structure interface differs from the motion that would occur at this point in the free field if the structure were not present, there is soil-structure interaction. If the interface moves or distorts differently than the corresponding surface in the free field, there is interaction. Average horizontal and vertical translation, rocking about a vertical axis are all included in the definition.

The solution to this type of problem can be approached in three steps.

They are:

1) Define movements of the ground surface

2) Characterize the interface between the earth and the structure

3) Predict the resulting movements in the structure

4) Iterate, as structural loads influence ground movements.

Earth-structure interaction problems are generally not well understood.

This study is focused on defining the movements of the ground surface due to sinkhole subsidence. The use of profile functions, an empirical method of subsidence prediction, is investigated and evaluated.

1.3 Note on Units

Every effort was made to present measurements using the System Internationale (SI), or metric system. However, due to equipment limitations all field work was accomplished using the English system of measurement. Consequently, in the text field measurements are reported in English units, with the metric equivalent following in parenthesis. No attempt at conversion was made for site maps, this aspect is most notable in Appendix A, Sinkhole Topographic Maps.

CHAPTER 2 LITERATURE REVIEW

2.1 Karst

The word karst is derived from the name of a limestone plateau in Yugoslavia. Characteristics of a karst region are numerous surface depressions, disruption of surface drainage, as well as caves, and other subsurface voids. Fundamental to the development of these features is underlying thick, carbonate rock susceptible to solution by water. The solution process is the reaction of the rock, water, and carbon dioxide to form dilute carbonic acid (Kemmerly, 1980).

Solution occurs along bedding planes, joints, and fractures in the rock that permit and are enlarged by the flow of water. Flow into and along discontinuities results in a highly irregular bedrock and soil overburden interface. Features of this interface are pinnacles, chimney-like openings in the rock, and the flow both of water and soil overburden into the subadjacent voids. The latter is believed to be the most common cause of sinkholes, (Beck, 1984; Newton, 1984; Kemmerly, 1980).

A sinkhole, or doline, is a closed topographic depression formed by the subsidence of the surface due to karst processes. Beck (1984) suggests classification of sinkholes by their mechanism of collapse. These classification would be:

1) Solution sinkholes formed from the slow dissolution of bedrock

2) Collapse sinkholes which arise when the roof of a bedrock cavern collapses

3) Subsidence and cover-collapse sinkholes formed by the piping or erosion of the soil overburden into a solution enlarged discontinuity.

Figure 2.1 illustrates the formation of a cover-collapse sinkhole. Sinkholes formed by movement of the soil overburden into solution channels in the bedrock, and the subsequent deformation of the induced soil cavity or void, are believed to be the primary causative mechanism of subsidence in locations studied. Chen and Beck (1989), on the relative importance of insitu gravitational forces to hydraulic forces in the formation of sinkholes and deformation of the surface, state that:

> Gravitational movement of overburden sediment down into voids in the limestone is a major factor in sinkhole development. This causes soil cavities which stope toward the surface. The flow of water is not necessary to cause the development of a sinkhole.

Figure 2.2 illustrates the resulting surface expression of these features.

2.2 Profile Functions

Empirical methods have long been used to predict subsidence above longwall coal mines. One method of empirical subsidence prediction, which may have application in karst terrain, is the use of profile functions.

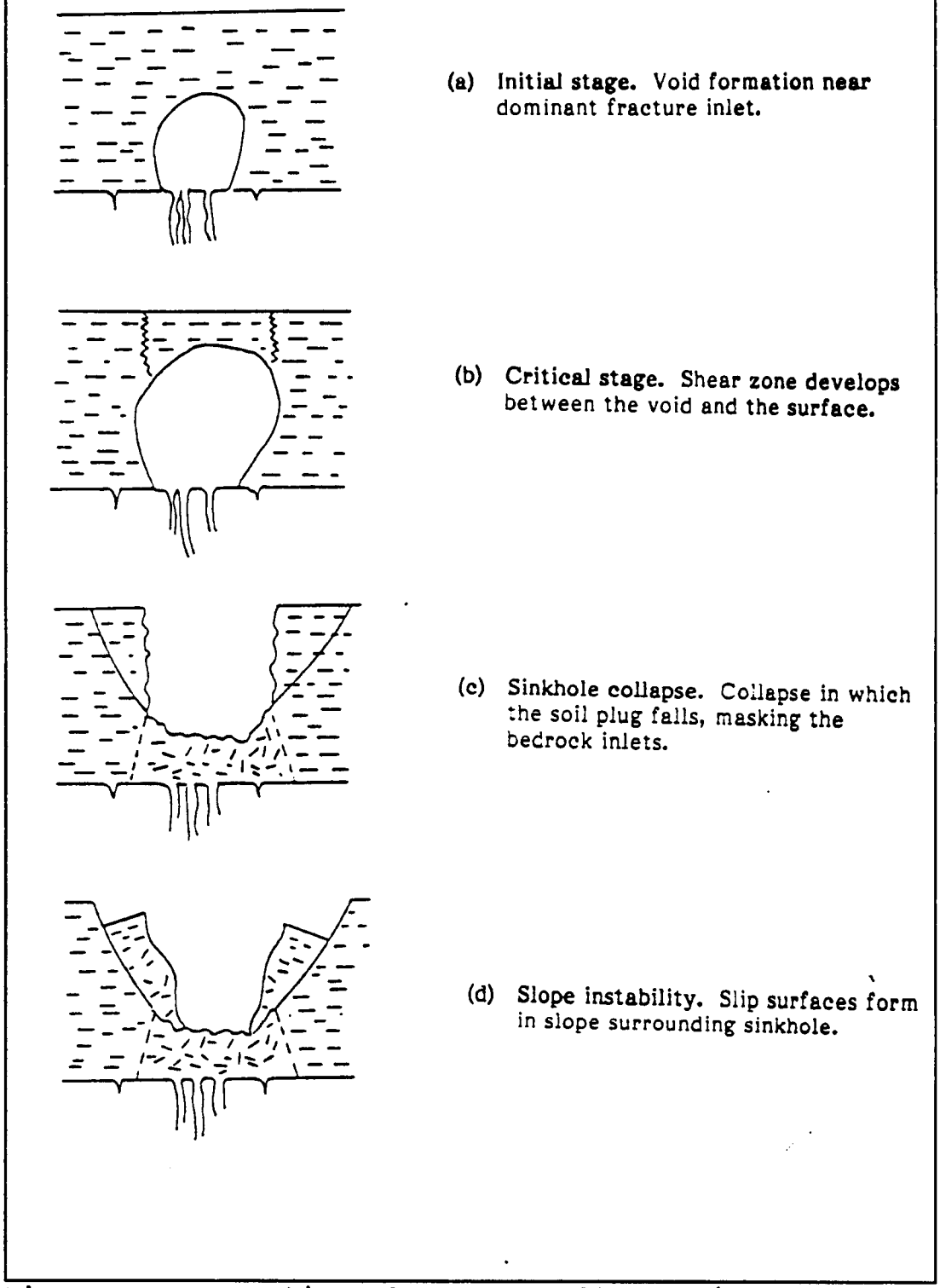
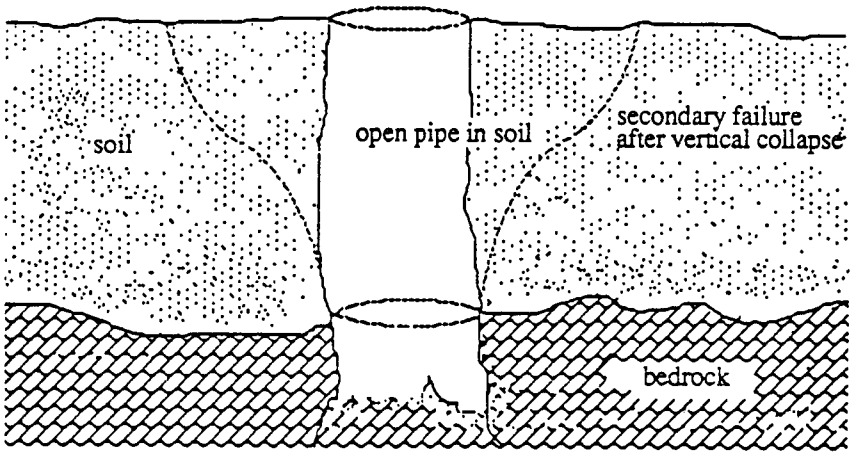
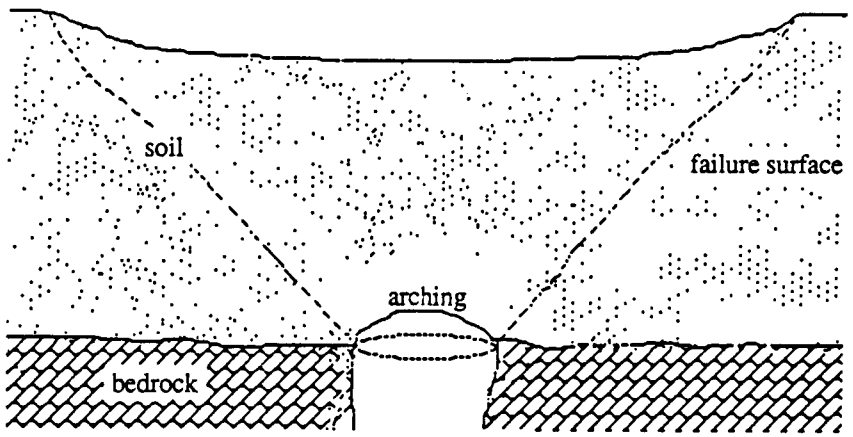


Figure 2.1 Formation of a cover-collapse sinkhole, and secondary slope failure (after Beck, 1984; Ogden, 1984)



a) Open Karst Pipe



b) Saucer - Shaped Sink

Figure 2.2 Surface expression of sinkholes due to the deformation of a subsurface void (Yoon, 1987)

Originally developed in Europe, profile functions predict subsidence, or rather predict the shape of the induced basin, by assuming that similar conditions, geometry, and material properties, will induce a similar response at the surface. Application of this method involves fitting a mathematical function to a significant number of actual subsidence basin profiles. The curve fit determines constants that predict and describe the shape of a subsidence basin. The lateral and vertical magnitude of the surface deformation is determined by subsurface geometry, as is elaborated below.

Table 2.1 is a listing of several profile functions that have found application in subsidence prediction. These functions can generally be separated into those which produce symmetric profiles and those which do not. Two functions have found application in the Appalachian coal fields of the United States: 1) the hyperbolic tangent function, which requires symmetry and 2) the negative exponential function, which is not symmetric. Both functions have been shown to accurately describe subsidence basins.

2.2.1 The Hyperbolic Tangent Function

Use of the hyperbolic tangent function in subsidence prediction in the United States was first suggested by Brauner (1973). The function is symmetric about the inflection point of the profile. The inflection point is

Table 2.1 Profile functions (Chen and Peng, 1981).

Function	Origin
$\frac{S(x)}{S_0} = 1 - Z + \frac{1}{2\pi}\sin(2\pi Z)$	Kolbenkov (Russian)
$\frac{S(x)}{S_0} = (1-Z)^{4.54}\, e^{4.54Z}$	Avershin (Russian)
$\frac{S(x)}{S_0} = e^{\frac{-x^2}{2B}}$	Moto (Hungarian)
$\frac{S(x)}{S_0} = -1 \int_x^{\infty} e^{\frac{-\pi x^2}{r^2}}\, dx$	Knothes (Poland)
$\frac{S(x)}{S_0} = \frac{1}{2}\left[1 - \tanh \frac{6x}{H}\right]$	Wardell (British)
$\frac{S(x)}{S_0} = \frac{1}{2}\left[1 - \tanh \frac{2x}{H \cot B}\right]$	King and Whetton (British)

where $Z = X/L$, and $r = H \cot B$.

defined as the location on the curve at the point of one-half the maximum vertical subsidence, as shown in Figure 2.3. The function is of the form:

$$S(x) = \frac{1}{2} S_o \left(1 - \tanh \frac{C X}{B}\right) \qquad [2.1]$$

where $S(x)$ = vertical displacement, S_o = maximum vertical displacement, X = horizontal distance from the origin, B = horizontal distance from the centerline to the point of inflection, and C = the empirical parameter.

The hyperbolic tangent can also be expressed as:

$$\tanh X = \frac{\sinh X}{\cosh X} = \frac{e^{X} - e^{-X}}{e^{X} + e^{-X}} = \frac{e^{2X} - 1}{e^{2X} + 1} \qquad [2.2]$$

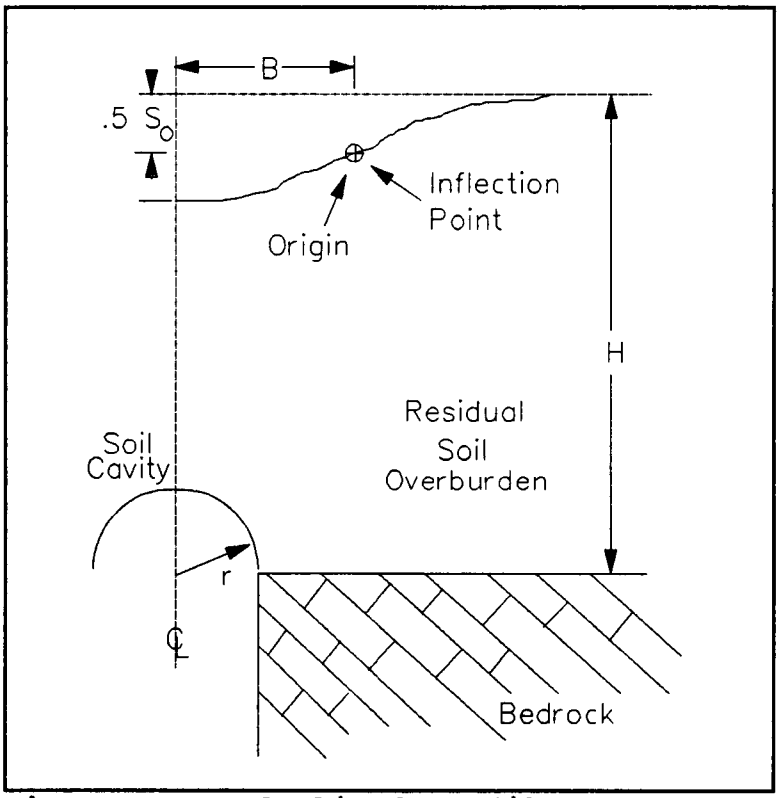


Figure 2.3 Idealized profile and definition of terms for the hyperbolic function

The right hand side of Equation 2.2 is the form of the function used when fitting field and numerical profile data.

Figure 2.3 is a generic subsidence profile identifying the terms that define the hyperbolic tangent function, hereafter known as the hyperbolic function. The origin is located at the inflection point with positive values upward and to the right. The centerline of the profile is located at the point of maximum vertical displacement.

2.2.2 The Negative Exponential Function

The negative exponential function suggested for use in the U.S. by Chen and Peng (1981) differs from the hyperbolic function in that it is not symmetric about its inflection point, nor does it have the same location of its frame of reference or origin. The negative exponential function is:

$$S(x) = S_o \, e^{-\alpha (X/L)^{\beta}} \qquad [2.3]$$

where L = half-width of the subsidence basin, α & β are the empirical parameters, with other parameters as defined above for the hyperbolic function.

Figure 2.4 identifies the terms of the negative exponential function. The origin is located on the centerline of the basin at the point of maximum vertical displacement. The half-width of the basin is taken as the horizontal distance from the origin to a point on the

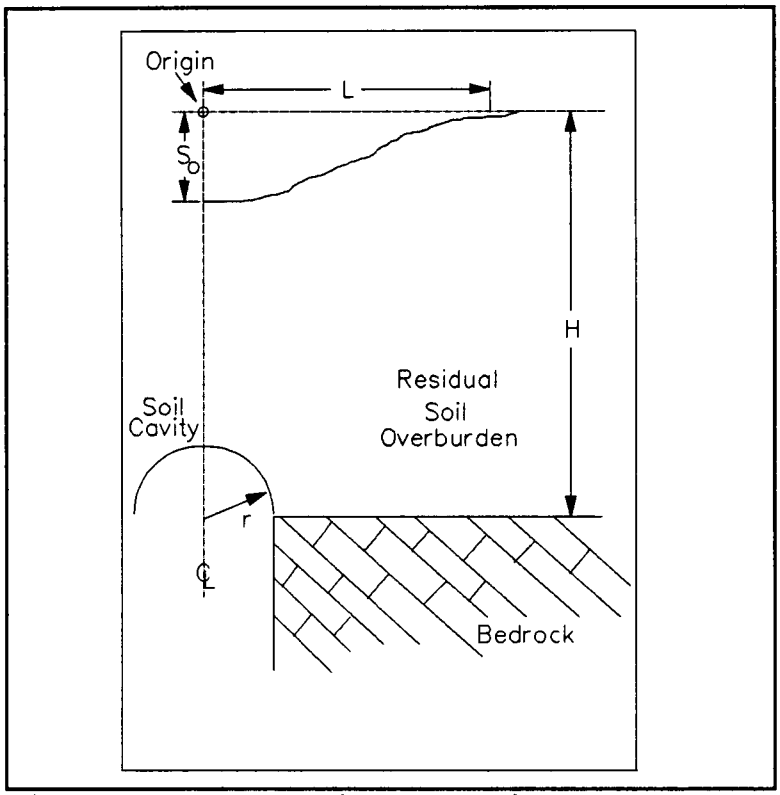


Figure 2.4 Idealized profile and definition of terms for the exponential function

surface where there is no vertical displacement. This function is hereafter referred to as the exponential function.

It is common practice, with both functions, to normalize vertical displacement by its maximum value. Horizontal distances are also often normalized by the distance(s) to the origin. This preserves the relative shape of the curve, while neglecting magnitudes.

2.2.3 Slope and Curvature of Profile Functions

The slope at any point on a curve is the first derivative of its function, and the curvature is the second derivative. Vertical displacement, slope, and curvature can be associated with structural distress. For the hyperbolic function the profile is given by:

$$f(x) = S(x) = \frac{1}{2} S_0 \left[1 - \tanh \frac{C X}{B}\right] \quad [2.4]$$

The slope of the profile is:

$$f'(x) = i(x) = -\frac{1}{2}\frac{C}{B} S_0 \operatorname{sech}^2 \frac{C X}{B} \quad [2.5]$$

The curvature of the profile is:

$$f''(x) = k(x) = S_0 \frac{C^2}{B^2} \operatorname{sech}^2 \frac{C X}{B} \tanh \frac{C X}{B} \quad [2.6]$$

For the exponential function the profile is:

$$f(x) = S(x) = S_0 e^{-\alpha (X/L)^{\beta}} \quad [2.7]$$

The slope of the profile is given by:

$$f'(x) = i(x) = \frac{-S_0 \alpha \beta X^{\beta-1} e^{-\alpha (X/L)^{\beta}}}{L^{\beta}} \quad [2.8]$$

The curvature of the profile is:

$$f''(x) = k(x) = \frac{-S_0 \alpha \beta X^{\beta-2}}{L^{\beta}} \left[(\beta-1) - \frac{S_0 \alpha \beta X^{\beta}}{L^{\beta}} e^{-\alpha (X/L)^{\beta}} \right] \quad [2.9]$$

All variables have been previously defined in Sections 2.2.1 and 2.2.2. Figure 2.5 shows relative plots of slope and curvature versus normalized half-width for the exponential function.

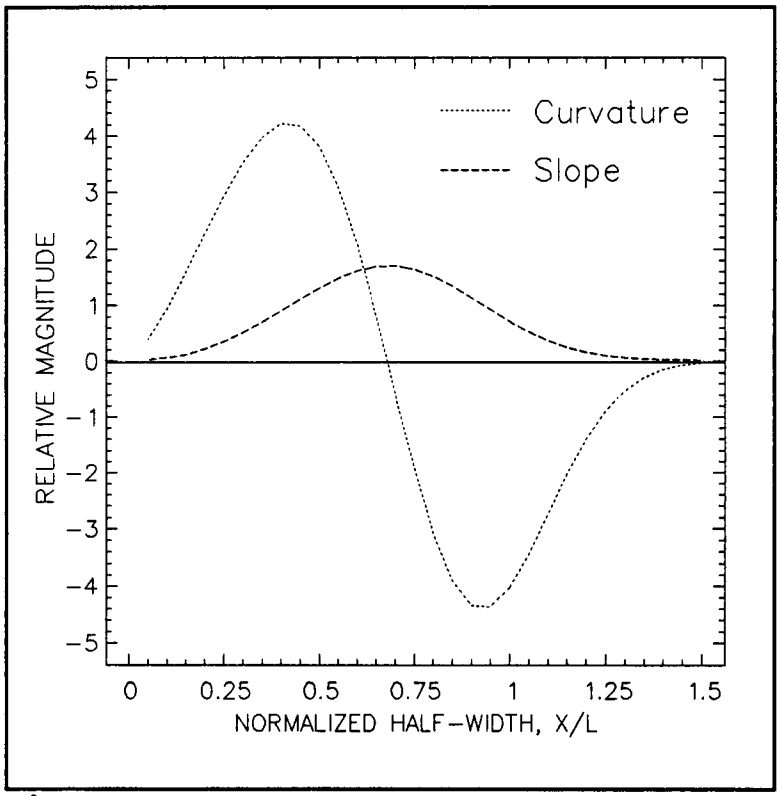


Figure 2.5 Plot of slope and curvature versus horizontal position

2.3 Magnitude and Extent of Subsidence

Application of profile functions for subsidence prediction requires knowledge of the subsurface geometry. Vertical displacement is related to the size and volume of a subsurface void, while the depth to the void and the overburden material control the lateral extent of subsidence. In longwall mining, the magnitude and extent of subsidence are related by the width-to-depth ratio, a ratio of the size of the void to the depth to the void. The subsurface geometry of a longwall mine often allows a width-to-depth ratio greater than one. A significant width-to-depth ratio permits derivation of an expression in terms of a single variable, typically the depth to the void.

Subsidence profiles above a longwall panel are typically described as having the characteristic shapes of subcritical, critical, or supercritical (Peng and Chaing, 1984). If the value of maximum subsidence for the basin occurs at a single point, usually at the center, and is less than the maximum possible subsidence the profile is subcritical. Critical profiles are similar in shape to subcritical profiles, but additionally, the magnitude of subsidence has reached its maximum possible value. If the basin has a flat bottom, having uniformly reached this maximum displacement, the profile is described as supercritical. The maximum possible vertical displacement is a function of the width-to-depth ratio.

Application of profile functions for subsidence prediction does not require knowledge of mechanical material behavior. The overburden material is typically assumed to be homogenous, even when this is not entirely correct. Karmis et al. (1987) applies a reduction factor to the estimated maximum subsidence based on the percentage of competent strata above the subsurface void.

2.3.1 Angle of Draw

The study of subsidence above coal mines has spawned a plethora of terminology to define the lateral extent of subsidence. A review these is followed by definition of the angle of draw for this study.

Chen and Peng (1981) define four angle parameters: limit angle, angle of critical deformation, angle of break, and angle of complete mining. They are defined as:

1) The **limit angle** is the angle from the horizontal to a line connecting the edge of the subsurface void to the point of zero subsidence on the surface. Chen and Peng (1981) use this to calculate the radius of influence or half-width of the profile

2) The **angle of critical deformation** is the angle from the horizontal to a line connecting the edge of the subsurface void to the surface at the point to which certain structures may be subjected to damage

3) The **angle of break** is the angle between the horizontal to a line connecting the edge of the subsurface void to the point on the surface where the first tension crack occurs

4) The **angle of complete mining** is the angle between the horizontal to a line connecting the edge of the subsurface void to the outermost point of maximum subsidence at the surface, taking note of subcritical or supercritical subsidence relative to the centerline of the basin.

Karmis et al. (1987) uses two other angle parameters: 1) angle of draw, and 2) angle of influence, they are defined as:

1) The **angle of draw** is the angle between the vertical to a line connecting the edge of the subsurface void to the point of zero vertical displacement on the surface. This angle is similar to the limit angle, above (NCB, 1975)

2) The **angle of influence** is the angle between the horizontal to a line connecting the edge of the subsurface void at depth to the point on the surface where $S(x) = 0.0061\ S_o$.

The various angle parameters are intended to define the lateral extent of subsidence, and relate the lateral extent to the depth of overburden above a subsurface void, they do not define an explicit slip or failure surface.

Yoon (1987) in a plasticity based axisymmetric analysis of slip surfaces about an open karst pipe found non-linear slip surfaces. Their lateral extent was a function of the depth of overburden and cavity radius. However, they could be approximated by a planar slip surface oriented from the horizontal at:

$$45^\circ + \phi/2 \qquad [2.10]$$

where ϕ = the angle of internal friction. In effect, Yoon

(1987) defines an angle of draw with a line connecting the outer radius of an open pipe at bedrock and the emergence of a failure surface.

In this study, the angle of draw (δ) will be measured, with respect to the horizontal, from the centerline at bedrock as shown in Figure 2.6, instead of from the outer edge of the cavity, as in mining. This is conservative, from the standpoint of damage to a surface structure, and should underestimate the lateral extent of the subsidence

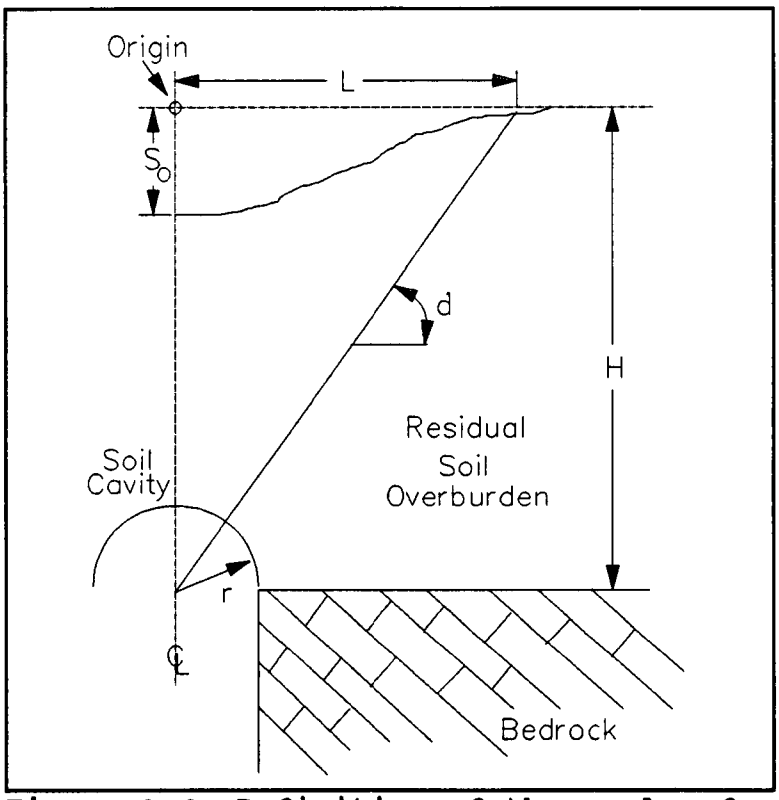


Figure 2.6 Definition of the angle of draw in terms of the depth of overburden and basin half-width

basin. For a given value of vertical displacement, an underestimated half-width will increase the slope and curvature of the profile. This definition is necessitated by the fact that the actual soil cavity radius can rarely be determined.

The relationship between basin half-width, L, and the depth of overburden, H, may be expressed in terms of the angle of draw, δ, from the triangle in Figure 2.6. The expression is:

$$\tan \delta = \frac{H}{L} \qquad [2.11]$$

2.4 Structural Damage Associated with Subsidence

Figure 2.7 illustrates the ground movements and induced loadings associated with subsidence. The rim of a subsidence basin is a zone of tension, and the bottom of the basin is subjected to compressive forces (Illinois Mine Subsidence Insurance Fund, 1987). This idealization is consistent with known ground movements associated with karst subsidence. For example, Newton (1976) and Wilson and Beck (1988) noted the existence of tension cracks around the location of later collapse.

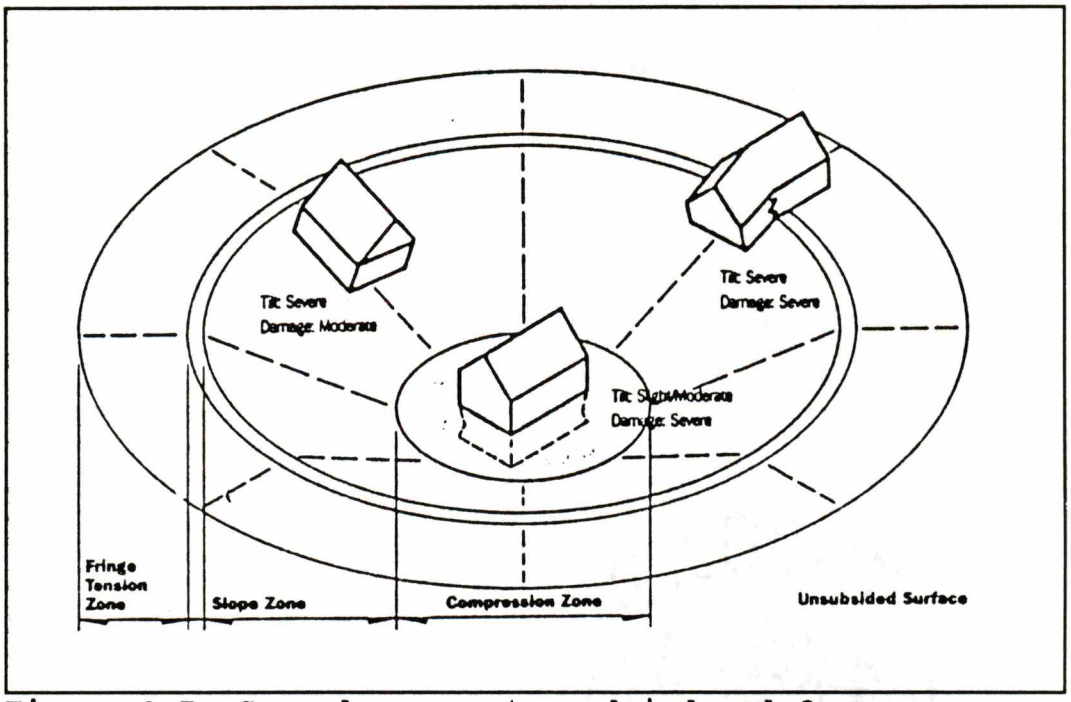


Figure 2.7 Ground movements and induced forces (Illinois Mine Subsidence Insurance Fund, 1987)

The movement induced by subsidence has five components:

1) Vertical displacement
2) Slope of the subsidence basin
3) Curvature of the basin
4) Horizontal displacement
5) Horizontal strain, relative to a surface structure.

Horizontal strain is the first derivative of horizontal displacement with respect to the horizontal.

Chen and Peng (1981) suggest a constant relationship between horizontal displacement and the slope of the subsidence basin:

$$d_h(x) = K\ i(x) \qquad [2.12]$$

where $d_h(x)$ = horizontal displacement, $i(x)$ = slope of the basin, and K = constant. K is determined in one of two ways. Using the average ratio method, the ratio of horizontal displacement to slope is determined at discrete points along the curve, and an average of the values is taken as the constant. The other method is the maximum ratio method whereby the constant has the value of the ratio of the maximum horizontal displacement to the maximum slope.

Alternatively, Karmis et al. (1987) suggested a constant relationship between horizontal strain and vertical curvature. This approach is very similar to above, in that:

$$\epsilon_h(x) = K\ k(x) \qquad [2.13]$$

where $\epsilon_h(x)$ = horizontal strain, $k(x)$ = vertical curvature of the profile, and K is a constant. Karmis et al. (1987) also suggests that K may be a function of the depth of overburden and the basin half-width.

2.4.1 Sanitary Landfill Liner Systems

Sanitary landfill liner systems are impermeable barriers intended to prevent the escape of leachate from a landfill into the ground water. Typically liner systems are one of two types, a compacted clay liner or a composite geotextile-geomembrane liner. In both cases the key criteria for determining failure is hydraulic conductivity,

or rather hydraulic permittivity, as determined by the liner system's intended use.

Figure 2.8 illustrates the generalized behavior of a liner system in the fringe tension zone around a subsidence event. The pores of a geotextile/geomembrane will likely be enlarged and allow increased permittivity. Permittivity is the parameter governing the rate of flow through a geotextile. It is equal to the rate of water flow through the geotextile per unit area and per unit hydraulic head

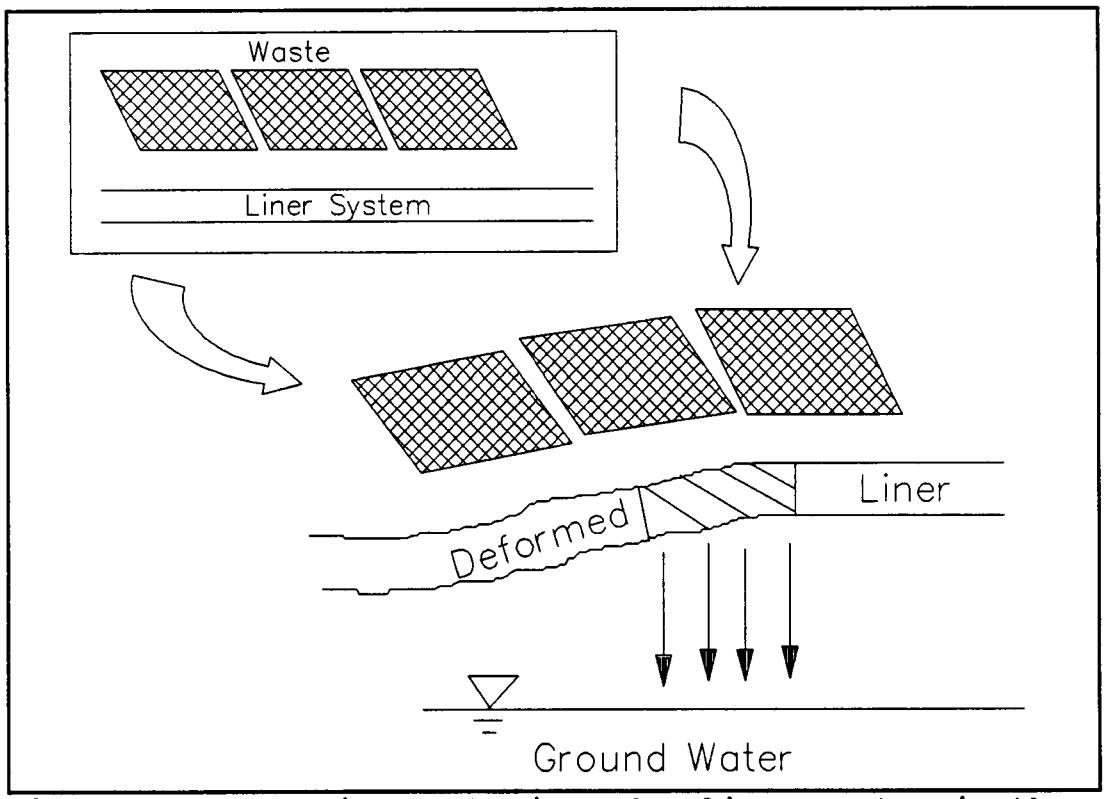


Figure 2.8 Idealized behavior of a liner system in the tension zone around a subsidence event

(Tensar, 1986). The Executive Subcommittee on ASTM D-35, Geotextiles, Geomembranes and Related Products, is preparing a draft standard for determining the permittivity of geotextiles under loading, but no recommendation is available (Suits et al., 1987).

2.4.2 Damage Criteria for Buildings

In case of subsidence or collapse, constructions on the surface will be subject to damage from the differential movements of soil and structure. Preliminary critical values for the extent of structural damage due to subsidence have been proposed. These are listed in Table 2.2.

Bhattacharya et al.,(1984) classified the structures damaged as:

1) Brick and masonry structures, block load bearing walls, and low rise structures

2) Steel and reinforced concrete frame structures

3) Timber frame structures

4) Massive structures of considerable rigidity or central core design.

Earth structures are not included in this classification.

Three levels of damage severity are proposed. The least severe, architectural damage, is characterized by small scale cracking and the sticking of doors and windows. Functional damage is identified by the instability of some structural elements, such as broken window panes, and a

restriction of some building services. The most serious level, defined as structural damage, is where the possibility of collapse is imminent and large scale rebuilding is required.

Table 2.2 Damage criteria for buildings (Bhattacharya et al., 1984).

Building Category Level of Damage	Angular Distortion ($x10^{-3}$)	Horizontal Strain ($x10^{-3}$)	Deflection Ratio ($x10^{-3}$)	Radius of Curvature (km)
Brick and Masonry				
Architectural	1.0	0.5	0.3	-
Functional	2.5 - 3.0	1.5 - 2.0	0.5	20.0
Structural	7.0	3.0	-	-
Steel and Reinforced Concrete				
Architectural	1.3	-	-	-
Functional	3.3	-	-	-
Structural	-	-	-	-
Timber				
Architectural	1.5	1.0	-	-
Functional	3.3 - 5.0	-	-	-
Structural	-	-	-	-
Massive, Rigid and Central Core				
Architectural	-	-	-	-
Functional	-	-	-	-
Structural	-	-	-	-

The five components of ground movement from subsidence have been distilled into damage-causing parameters. The parameters are (Bhattacharya et al.,1984):

1) **Angular distortion** is the angular rotation of a line connecting two observation points minus the rigid body rotation

2) **Horizontal strain** where tensile strains are generally more harmful to buildings and cause cracking. Compressive strains may cause buckling of a structure

3) **Deflection ratio** is indicative of the bending deformation, and is defined as the maximum displacement from a line connecting two observation points

4) **Radius of curvature** is the inverse of curvature, and may be calculated in one of two ways. First, the change in rotation divided by the observation interval or, secondly, directly from the second derivative of the profile function.

Horizontal ground movements are not examined in this study.

Damage to structures above a subsidence event is a function the type of structure and the location and orientation of the structure relative to the basin.

CHAPTER 3 METHODOLOGY

3.1 Site Description

The approximately 400 acre East Chestnut Ridge Site is located near the southeast end of the Department of Energy Oak Ridge, Tennessee Reservation. Figure 3.1 shows the location of the site. The site is within the rectangle defined by the southwest corner at N 24,000 - E 57,000 and the northeast corner, N 28,000 - E 61,500. The northern boundary is more specifically defined by the Y-12 security perimeter, and the southern boundary by Bethel Valley Road. The eastern and western boundaries are defined by intermittent streams, in the west by McCoy Branch, and the stream to the east is unnamed. Kerr Hollow quarry is located at the southwest corner of the site.

The topography of Chestnut Ridge is a composite of three discontinuous ridge lines separated by valleys containing local surface drainage. Typical relief between valleys and ridge crests is approximately 100 m. Karst subsidence features are located predominately along the ridges, aligned with strike, along possible joint sets, and along prominent photolinear features.

3.1.1 Geology

Chestnut Ridge is located near the western edge of the Valley and Ridge Physiographic Province of East Tennessee.

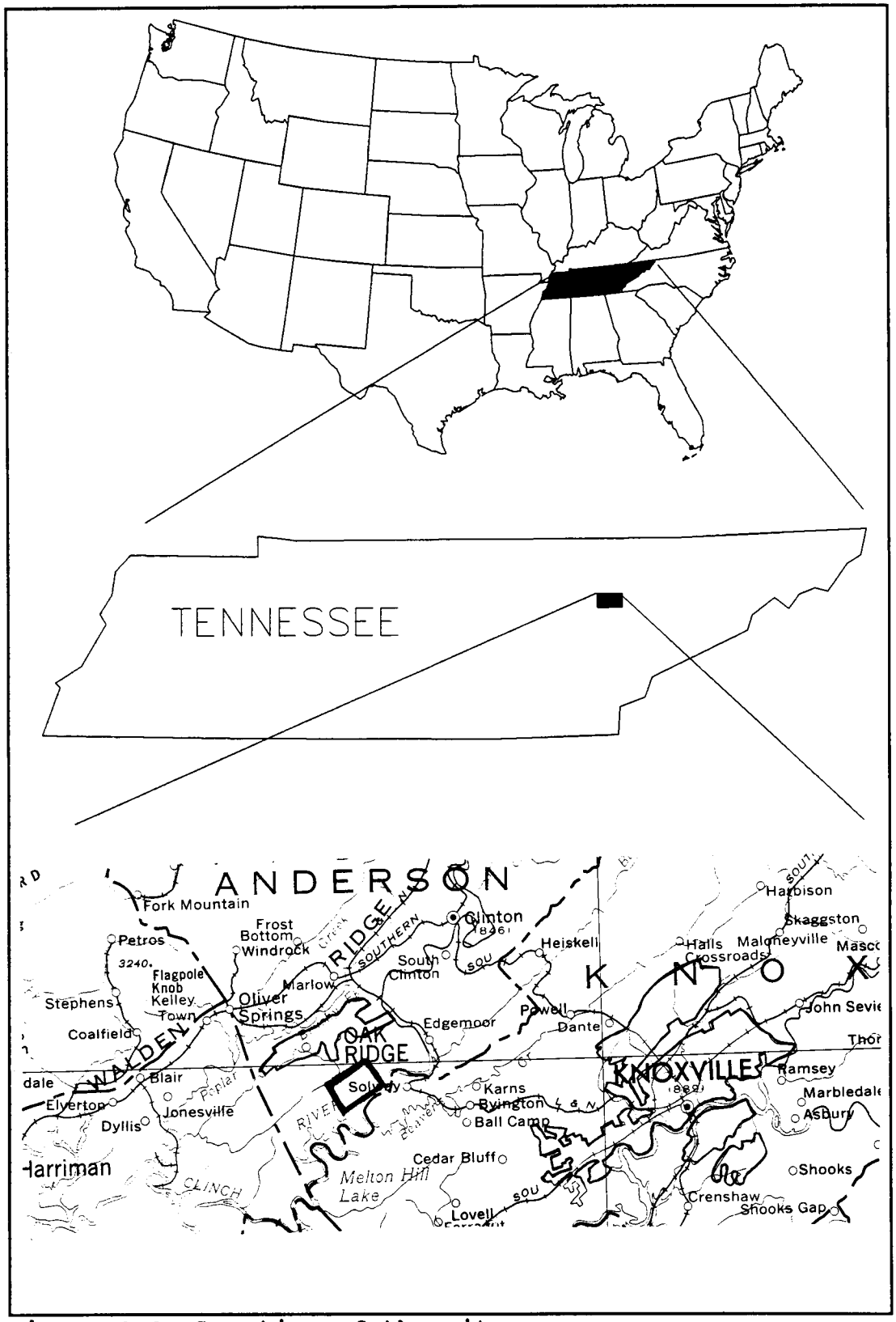


Figure 3.1 Location of the site

The Valley and Ridge Province is characterized by alternating valleys and ridges running southwest to northeast. This structure results from an arrangement of northeast trending folds, and thrust faults which dip to the southeast. The site is located on the Whiteoak Mountain thrust sheet, defined by the Whiteoak Mountain fault (Ketelle and Huff, 1984).

The site is underlain by carbonate rocks of the Knox Group, these are of Upper Cambrian to Lower Ordovician age. Rocks of the Knox Group are known for their susceptibility to the formation of karst features. Formations within the Knox Group occurring at the site, from north to south, and bottom to top stratigraphically, are the Copper Ridge Dolomite, Chepultepec Dolomite, Longview and Newala Formations. Myers (1982) describes each formation, from younger to older. They are:

> The Longview Dolomite consists of a very fine crystalline, light grey dolostone. This formation contains abundant chert. It weathers to a yellowish-brown to yellowish-red soil with moderate chert content. The thickness of this formation is 60 to 90 meters.
>
> The Chepultepec Dolomite is a fine- to medium grained, light grey dolostone with moderate chert with some beds of medium grained limestone. Weathered red to yellowish-red soils are typically sandy at depth. The thickness of this formation is 75 to 140 meters.

The Copper Ridge Dolomite consists of dark crystalline, knotty dolostone interbedded with thin beds of light grey, fine grained dolostone which has thin asphaltic layers. Upon weathering this formation produces large amounts of porous and non-porous chert which weathers into small angular chips and yellowish-brown to yellowish-red soils . The thickness of this formation is 200 to 300 meters.

While each formation is similar, the underlying rock influences the physical properties of the residual soil overburden. Myers (1982) proposes three tentative conclusions in this regard: First, soil color is related to the parent rock and is somewhat indicative of hydraulic conductivity. Darker red, clay soils tend to have a lower coefficient of hydraulic conductivity than do the more yellowish-red, clay soils. Second, soil color also correlates with plasticity, with the more yellowish-red clays having a higher plasticity index. Third, chert content is related to the parent rock, and shear strength increases with chert content. The higher the clay content by weight, the lower the angle of internal friction, and the higher the cohesion.

3.1.2 Soil Properties

Thirteen hollow stem auger borings made at the East Chestnut Ridge site yielded standard penetration test (SPT) and Shelby tube samples for testing. Tests to determine index properties included natural moisture content, unit weights, grain size distribution, and Atterberg limits,

(Geologic Associates, 1989). Soils are generally fine grained with 87.8%, 36 of 41 samples, having greater than 50% by weight passing a #200 sieve. Figure 3.2 shows that the percent-by-weight passing a #200 sieve does not vary significantly with elevation above bedrock, with most values between 55% and 85% passing a #200 sieve.

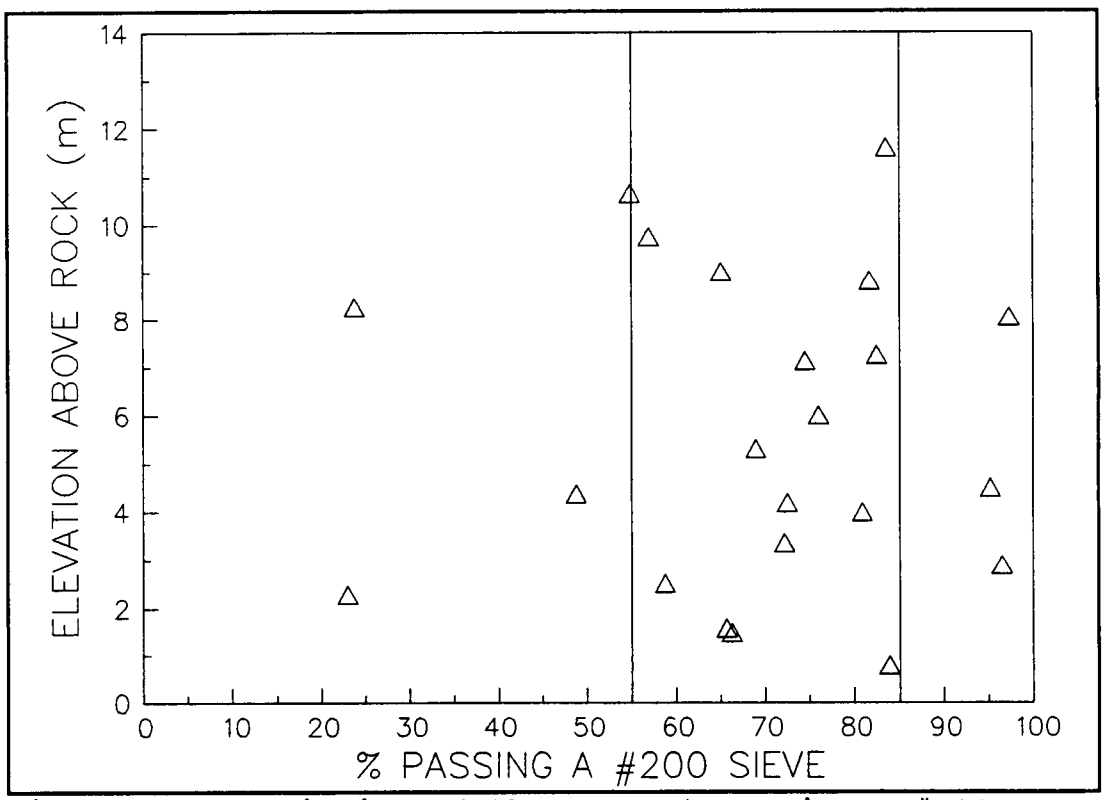


Figure 3.2 Variation of the percent passing a #200 sieve with elevation above bedrock

Figure 3.3 is a bar chart showing the frequency of categories for the Unified Soil Classification System, and suggests significant variation in classification. However, Figure 3.4 shows data for the same samples plotted on Casagrande's Plasticity Chart; all samples plot along the A-Line. This suggests little variation in soil types, at least within the recognized variability of the test procedure. Kulhawy (1983) suggests a variability of up to 20% in tests to determine Atterberg Limits. This plot is also consistent with Myers' (1982) work. The lack of variation in plasticity and gradation suggest the soil is relatively homogeneous at all depths, varying only in moisture content.

Figure 3.5 shows that liquidity index (LI) tends to increase near the bedrock surface. The liquidity index is a measure of whether a soil will behave as a brittle solid, a plastic, of even as a liquid. If the LI is less than zero the soil will behave as a brittle solid. If the value is between zero and one, then the soil will behave like a plastic. A LI greater than one indicates a viscous liquid. Figure 3.5 shows plastic behavior near the soil-bedrock interface.

Well tests at the West Chestnut Ridge Site (Woodward-Clyde, 1984; Myers, 1982) give field values for hydraulic conductivity with an order of magnitude of 10^{-6} cm/sec, with laboratory values generally one to two orders of magnitude

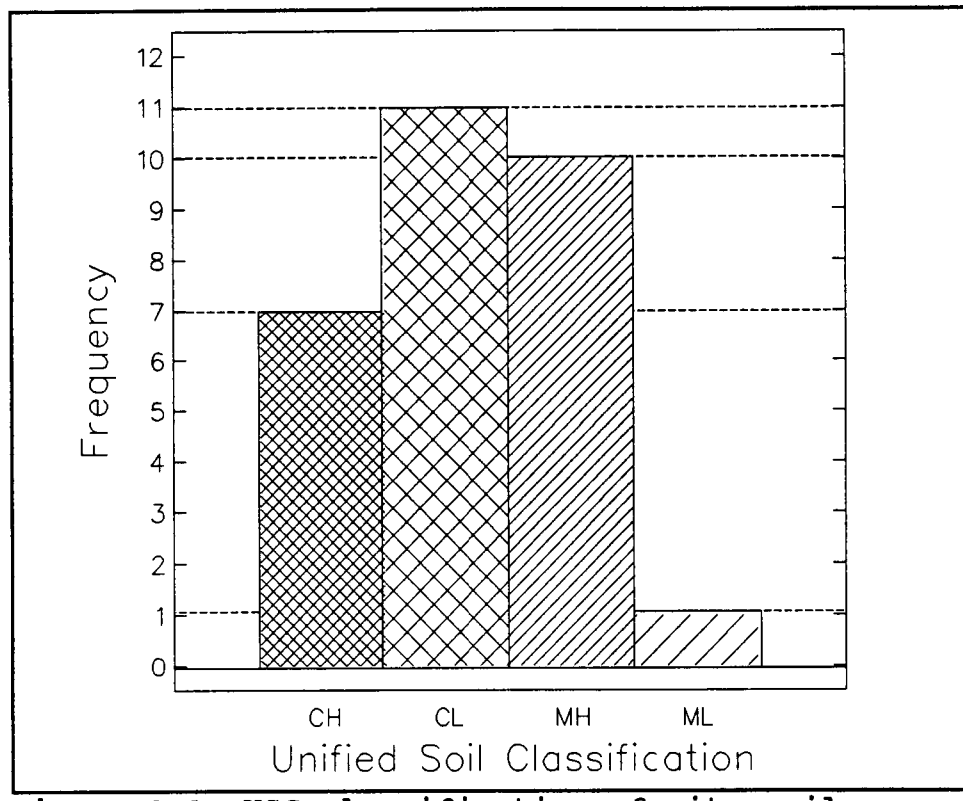


Figure 3.3 USC classification of site soils

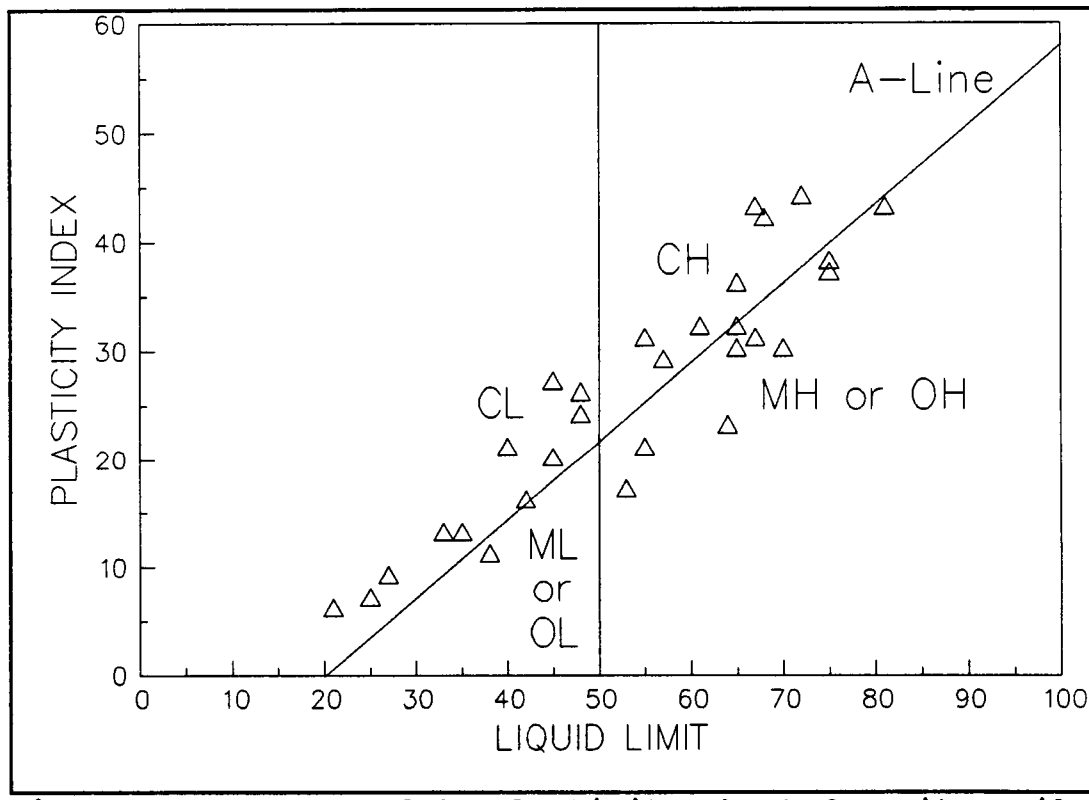


Figure 3.4 Casagrande's plasticity chart for site soils

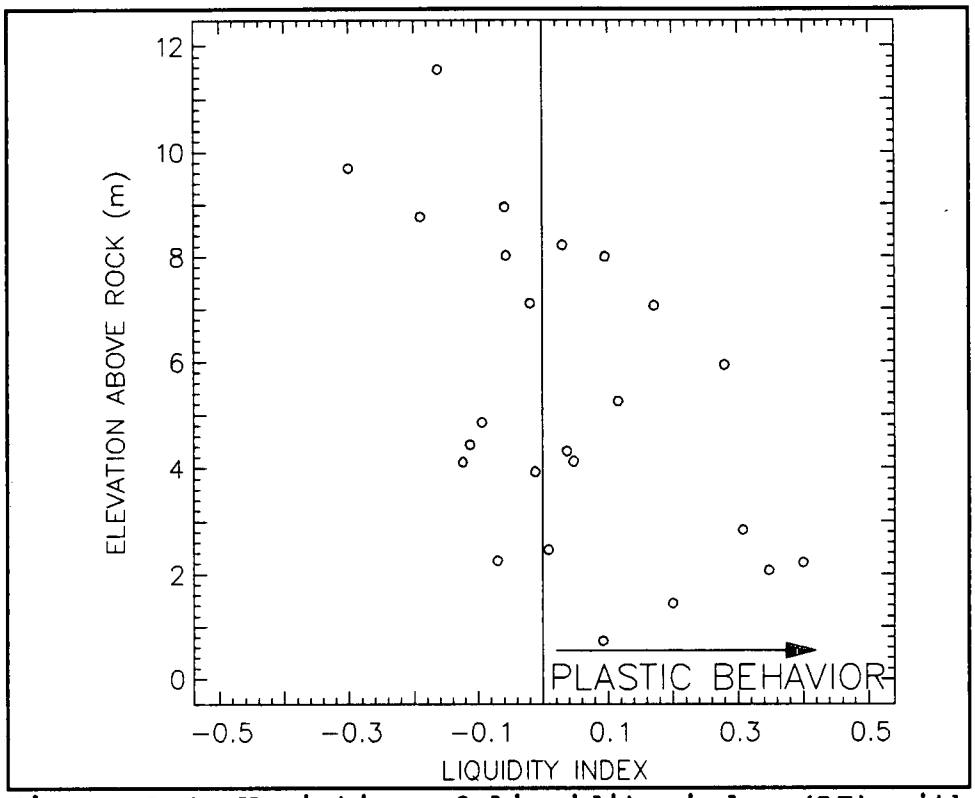


Figure 3.5 Variation of liquidity index (LI) with elevation above bedrock

less. A soil with a hydraulic conductivity on the order 10^{-7} cm/sec is generally considered impermeable. This has implications in sanitary landfill site selection.

Drained and undrained triaxial tests were conducted to determine soil shear strength and behavior under load, (Geologic Associates, 1989). In addition, the hydrostatic response was obtained to determine parameters for advanced elastic and elastic-plastic numerical analysis, (Drumm et al., 1989).

The drained parameters, ϕ = 18.6° and c = 15.8 kPa, were measured for soils on the East Chestnut Ridge site. These are below the values determined for West Chestnut

Ridge with, ϕ = 23°, and c = 31.6 kPa (Woodward-Clyde, 1984). Both sets are within the range reported by Myers (1982) for residual soils of the Knox Group.

3.2 Field Methods

In excess of 20 sinkhole-like features are located on site, 11 of these were selected for survey. The criteria for selection were: collapse, topographic closure, significant diameter, unmodified natural origin, and accessibility. Sinkholes were numbered in the order they were surveyed. Sinkholes 01 thru 05 were adjacent and located on the northern ridge, 06 and 07 were on the intermediate ridge, and 08 thru 11 were on the southern ridge, as shown in Figure 3.6. Of these 11, Sinkhole 05 was the only cover-collapse feature.

3.2.1 Profile Selection

Ten karst features provided the field data for profiles, the cover-collapse feature was not included. The primary common characteristics of these 10 features were continuous profiles, significant size, and accessibility. Differential leveling, a common technique of plane surveying, was used to determine the elevation of points within each feature. Plane surveying neglects the spheroidal shape of the earth and assumes that its mean surface is a plane. Differential, or direct leveling, is a method for determining an unknown elevation at a point



Figure 3.6 Location of sinkholes on the East Chestnut Ridge site

relative to another point of known elevation within the line of sight. All surveying and mapping was done in the English unit of feet. Elevations were plotted and contours were manually interpolated to produce 1:120 scale (1 inch = 10 feet), 1 ft (0.3 m) contour interval topographic maps. Appendix A contains reductions of the original maps.

3.2.2 Survey Equipment

The equipment used in leveling was a dumpy level and a Philadelphia rod graduated to hundredths of a foot. Horizontal distances were measured with a 150 ft (45.72 m) add-type steel tape, also graduated to hundredths of a foot. A Brunton compass such as that used to measure strike and dip, was used to determine the orientation of level lines. Angles can be measured to the nearest degree using a Brunton compass. No corrections to account for systematic errors in leveling, horizontal distances, or in angular measurements were made to the field data.

3.2.3 Survey Methods

A benchmark, the point of known elevation, was placed within or adjacent to a sinkhole. The benchmark was a 18 inch (45 cm) wooden stake driven into the ground to within 2 inches (5 cm) of its butt. The elevation of the benchmark was assumed as 100 ft (30.48 m). Backsites were taken with the rod resting on the butt of the stake. Elevations in sinkholes 01, 02, 03 and 04 were taken relative to the same

datum adjacent to sinkhole 01. Sinkholes 08, 09 and 10 also share a common datum.

A row of wooden stakes, equidistantly spaced at 10 ft (3.05 m) intervals, was driven into the ground to form a baseline. The orientation of the baseline was measured relative to magnetic north. Elevations were measured at 10 ft (3.05 m) intervals along a line normal to, and originating with, the baseline. The level line was laid out prior to measuring elevations. The tape was stretched along the level line and 10 ft (3.05 m) intervals marked. Intermediate spot elevations were made on slopes greater than 15%, and in areas of rapid change in slope. The result was a two-dimensional grid or net with known elevations at least every 10 ft (3.05 m). Figure 3.7 is an example of the survey net.

3.3 Data Reduction

Linear interpolation between measured, and now known, points of elevation in the grid allowed points of constant elevation to be determined. These points were connected to form a contour line. Smoothing to a curve was accomplished as the line was drawn. This process was repeated with contours representing integer foot elevations throughout the entire grid to produce a topographic map of the sinkhole.

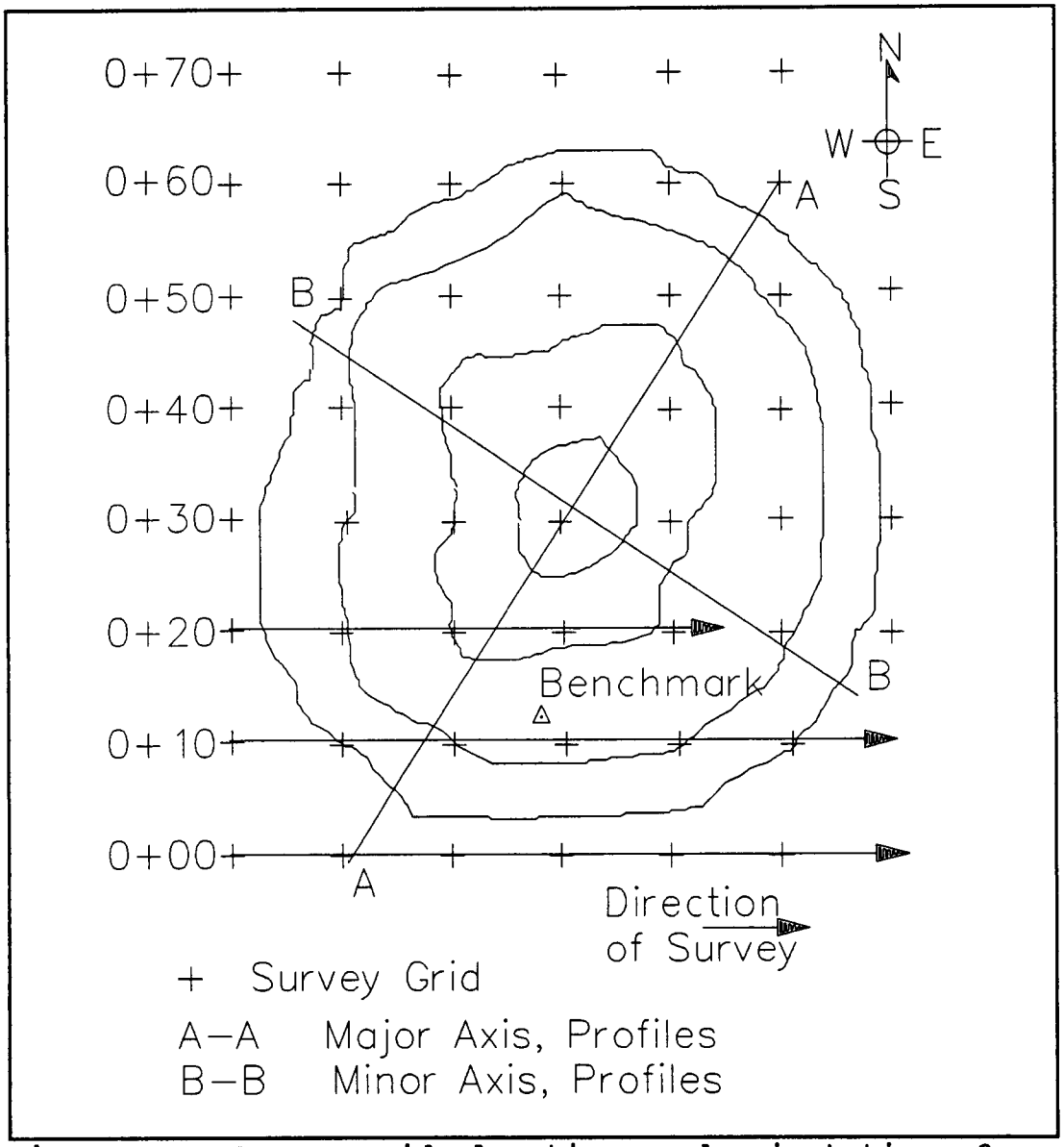


Figure 3.7 Survey grid, location, and orientation of the four profiles

3.3.1 Plan and Profile

Profiles were drawn using two criteria. First, the profiles were oriented along, and perpendicular to, the apparent major, or long, axis of the sinkhole. Secondly, the profiles were orthogonal to contour lines. Figure 3.7 also illustrates application of these criteria where A-A is the major axis, and B-B is the minor axis. The maps in Appendix A show the location and orientation of the selected profiles.

Application of the profile selection criteria yields 4 profiles per subsidence basin. Only 39 profiles were obtained from the 10 continuous subsidence basins. Sinkholes 06, 07 and 11 yielded only three profiles each, while sinkhole 10, because of its size and irregular shape, required six profiles.

Topography sloping at 5% to 10% and adjacent cut-and-fill complicated determination of the lateral extent of subsidence. Two different approaches were taken to deal with the problem. First, rotation of the profile about a horizontal axis to eliminate the effect of the adjacent slope distorted the location of maximum subsidence for flat-bottomed profiles and thus the shape of the profile. Alternatively, a cutoff for the lateral extent of subsidence was assumed to occur at 5% of the maximum vertical displacement. This approach is consistent with Karmis et. al. (1987). The latter method eliminated much of the effect

of adjacent slopes while preserving the natural shape of the basin, and was consequently used.

Discrete values of elevation and distance from the profile origin were resolved at irregular intervals which did not exceed 3.05 meters. The profile origin was assumed consistent with the frame of reference for the exponential function. Profile data consisted of the magnitudes of maximum subsidence and half-width and normalized elevations and distances.

3.3.2 Determination of Empirical Parameters

Regression to determine the fit of a nonlinear function to given data via a least squares estimate was accomplished using **STATGRAPHICS** (STSC,1988). Appendix B gives the geometric (L and B) and empirical (α, β, and C) parameters for all 39 field profiles from the fit of both functions, exponential and hyperbolic.

The exponential function and profile data were readily fit, as the data was maintained in this frame of reference with the origin at the point of maximum subsidence on the centerline of the profile. Figure 3.8 shows normalized field data from all 39 profiles and the associated best fit of the exponential function. The fit was good, with the square of the correlation coefficient R^2, equal to 0.926 for $\alpha = 2.50$ and $\beta = 3.30$. This method of fitting all 381 data points to a single curve is in contrast to Chen and Peng

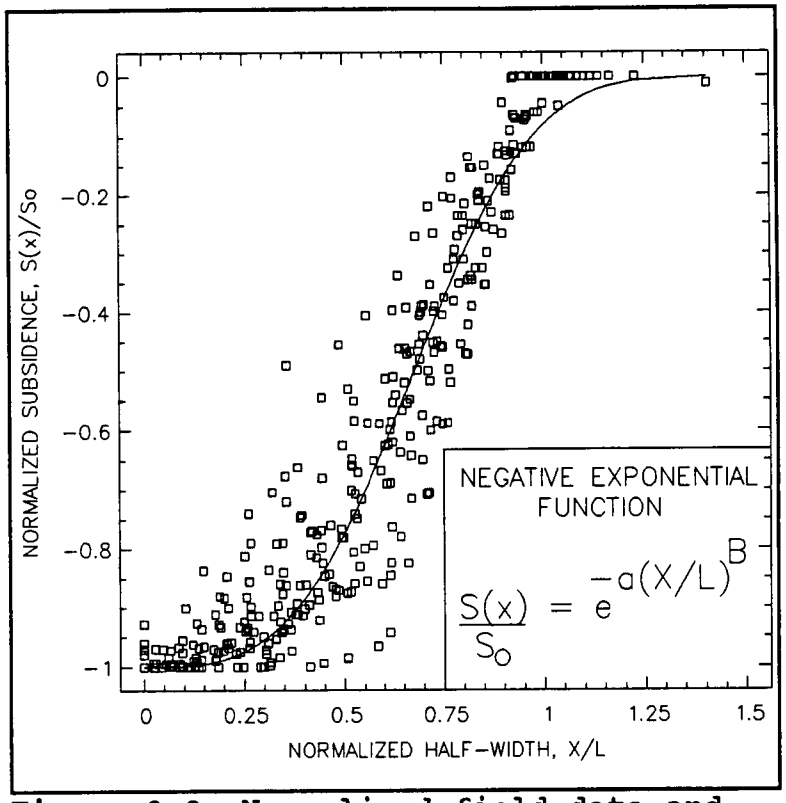


Figure 3.8 Normalized field data and best fit of the exponential function

(1981) who averaged the parameters from each of only six profiles.

Fitting the hyperbolic function to the data required a transformation of the data to move the origin to the inflection point. Figure 3.9 shows normalized field data from all profiles and the associated best fit curve, giving a value for C = 2.63. At first glance, the fit of the hyperbolic function appears better. A value for R^2 equal to 0.967 supports this. This excellent fit is due to the function's enforced symmetry about the inflection point.

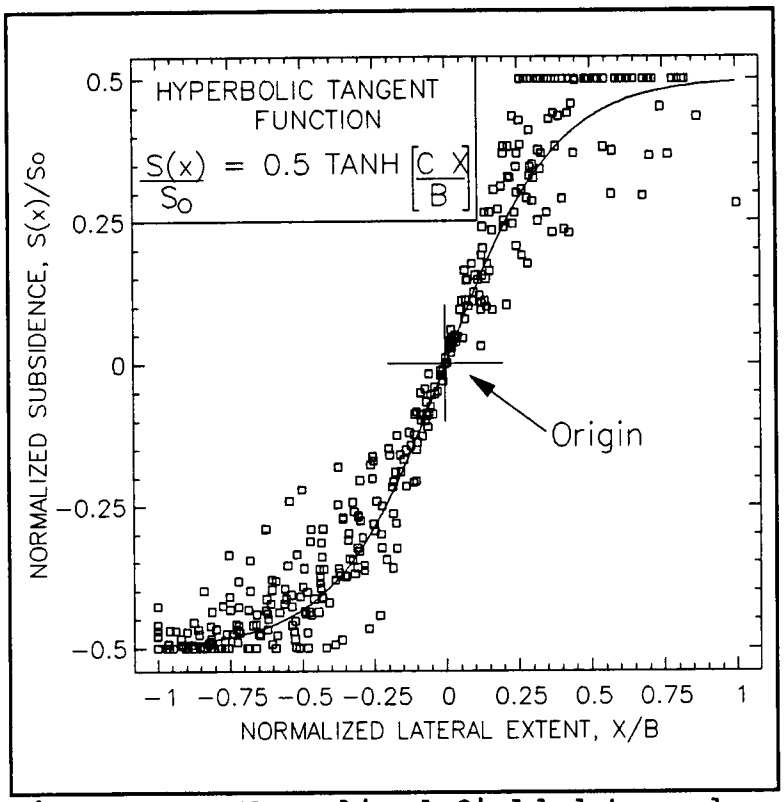


Figure 3.9 **Normalized field data and best fit of the hyperbolic function**

CHAPTER 4 RESULTS

4.1 Profile Functions and Profiles

Both the hyperbolic and exponential profile functions can be accurately fit to the field data. The latter has several advantages, notably, the exponential function provided a better fit to 34 of 39 field profiles. Also, the apparent distortion of normalized profiles is less with the exponential function, as symmetry is not forced. In addition, the half-width of a subsidence basin appears a more significant parameter and easily visualized, in defining the lateral extent of deformation, than the location of the inflection point. And finally, data reduction is more difficult with the frame of reference, that is, the origin at the inflection point.

The empirical parameters in both functions determine the shape of the profile. Figures 4.1 and 4.2 are comparisons of the parameters that define the shape of each function. C is the sole shape parameter in the hyperbolic function. The significant linear relationship between C and β in Figure 4.2, $R^2 = 0.990$, indicates β controls the shape of the exponential function. In the exponential function, β controls the relative shape, while α controls the flatness of the profile. The hyperbolic function has the advantage of only a single empirical parameter to describe the shape of the profile.

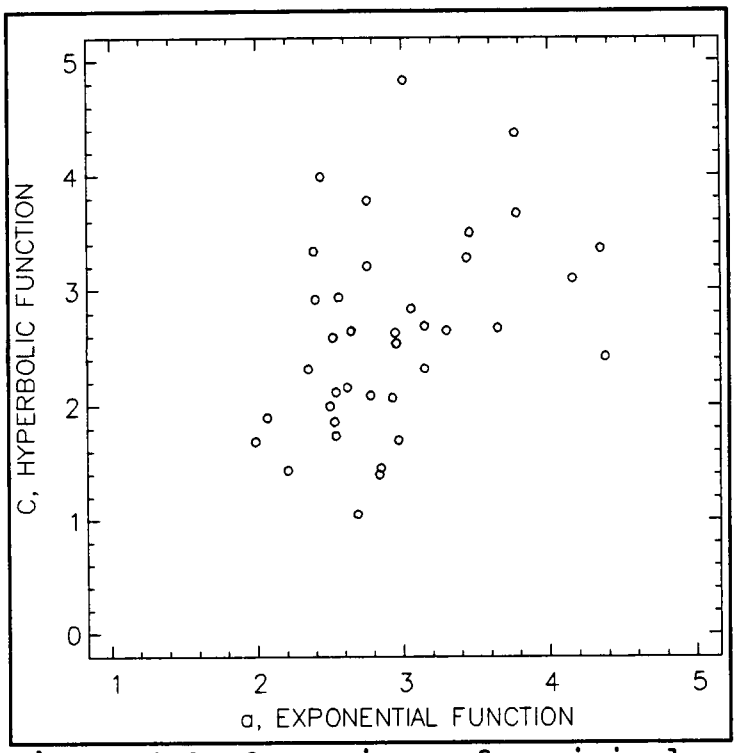


Figure 4.1 Comparison of empirical parameters, C and α, from field profiles

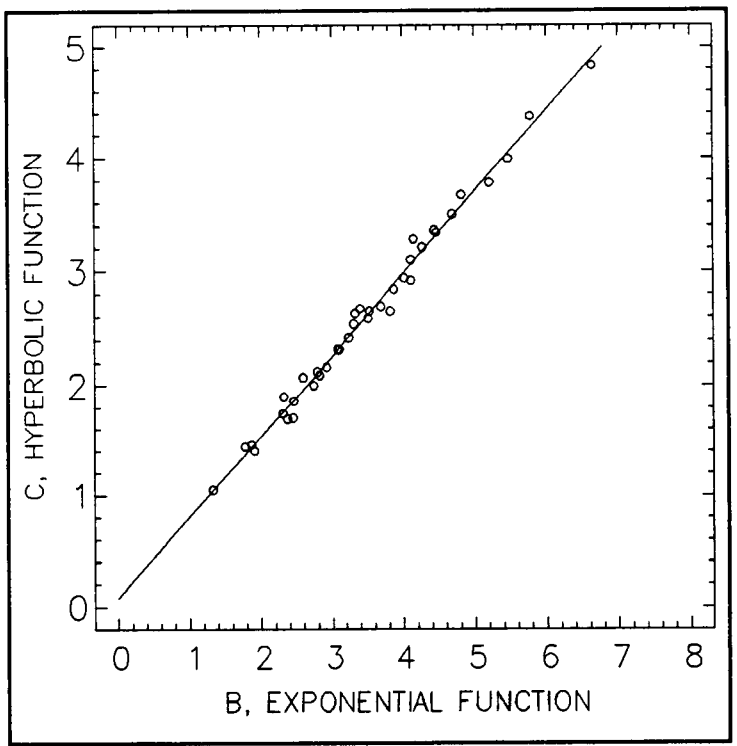


Figure 4.2 Comparison of empirical parameters, C and β, from field profiles

4.1.1 Subsidence Prediction from Field Profiles

The magnitude of the lateral extent and vertical displacement are determined by S_0, L, and B, and can be measured in the field to determine a range of likely values. The average maximum subsidence at the site was 2.07 m with a standard deviation of 1.37 m, over a range of 0.20 m to 5.40 m. The average half-width was 19.09 m with a standard deviation of 11.70 m, over a range of 5.85 m to 63.79 m. Soil borings provide an average depth to refusal, or depth to rock, of 28.58 m with a standard deviation of 9.95 m over a range of 12 m to 39 m.

A value for the angle of draw at the site can be determined from the depth overburden and basin half-width, as defined in section 2.3.1. This angle equals 56.3°. Generalizing the angle of draw as a case of active earth pressure. The angle of draw, δ, may be defined as:

$$\delta = 45^\circ + \phi/2 \qquad [4.1]$$

where ϕ = the angle of internal friction. Back calculation of ϕ for $\delta = 56.3^\circ$, yields $\phi = 22.6^\circ$. This value is within the range found by Myers (1982) for residual soils of the Knox Group.

For the 39 field profiles a significant relationship exists between L, the basin half-width, and B, the location of the inflection point. This relationship is shown in Figure 4.3. It can be expressed as a linear

equation, with $R^2 = 0.976$:

$$B = 0.75\ L - 1.34 \qquad [4.2]$$

where L and B are in meters. The intercept is small relative to the magnitude of L and can be neglected. This relationship infers that as the half-width of the subsidence basin increases, the basin maintains a flat-bottomed shape.

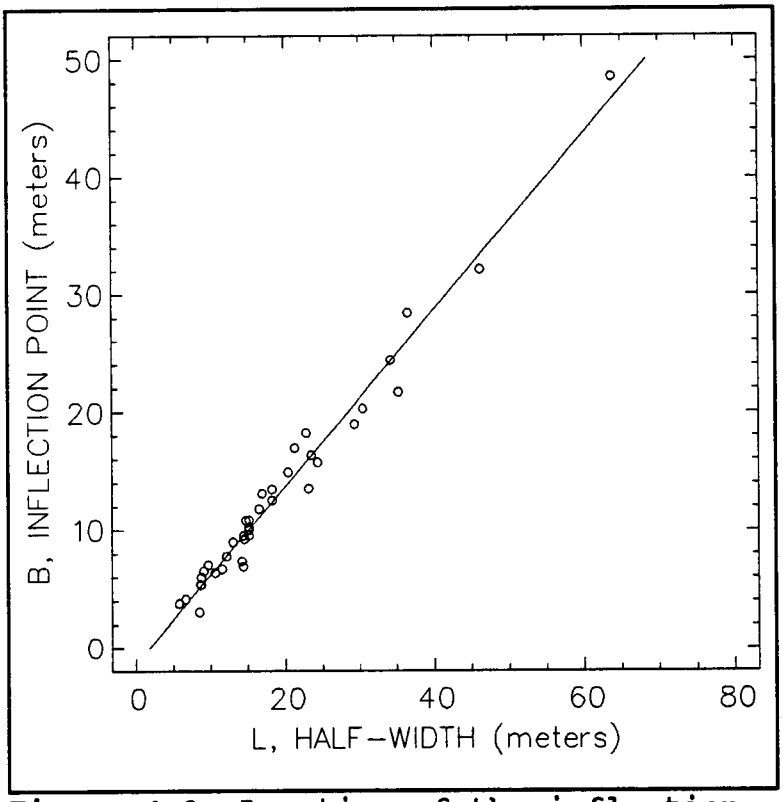


Figure 4.3 Location of the inflection point relative to basin half-width from the field data

The relationships expressed above, in Equations 4.1 and 4.2, provide the basis for developing predictive expression(s) for subsidence from the exponential and hyperbolic profile functions.

Direct substitution of Equation 4.1, angle of draw from soil internal friction angle, with Equation 2.11, angle of draw, into the exponential function, Equation 2.3, yields an expression for the vertical displacement at any point. This expression, with $\phi = 22°$, $\alpha = 2.5$, and $\beta = 3.3$ is:

$$S(x) = S_0 \, e^{-2.5 \left[\frac{X}{0.67\ H}\right]^{3.3}} \qquad [4.3]$$

where H is the depth of overburden in meters.

A similar expression can be derived for the hyperbolic function. The location of the inflection point is defined using Equation 4.2 from the basin half-width. The predictive profile function, with $\phi = 22°$ and the empirical parameter, C = 2.63, is:

$$S(x) = S_0 \left[1 - \tanh \frac{2.37\ X}{H}\right] \qquad [4.4]$$

where the variables are as defined above. S_0 remains an unknown and must be determined from field observations.

4.2 Idealization of Subsurface Geometry

Profile functions can only predict subsidence where

there is knowledge of subsurface geometry. Profile measurements do not, in themselves, convey information about the subsurface; correlation with actual conditions is required. Exploratory borings provide knowledge of the depth to bedrock, and samples to determine soil properties. They do not provide measurements of a void in the soil overlying an enlarged solution channel. Drumm et al. (1989) employed finite element analysis with both nonlinear elastic and elastic-plastic material models to make a parametric study of karst subsidence at the site. The surface and subsurface idealizations and soil models in the study provided insight into the relationship between the deformed profile at the surface and the geometry of soil and void below.

A series of 25 analyses were conducted to characterize the deformation of the soil and soil cavity into a subadjacent bedrock void. The behavior of the soil overburden was idealized with a hyperbolic, elastic, stress-strain model (Duncan and Chang, 1970) to represent the pre-peak, drained behavior of the soil.

For each finite element analysis, the cavity/residual soil system was idealized in two dimensions as plane strain. The finite element formulation utilized eight-node, isoparametric, quadrilateral elements (Ben-Hassine, 1987). The symmetric idealization of the soil-bedrock system is shown in Figure 4.4. All applied loading was due to insitu

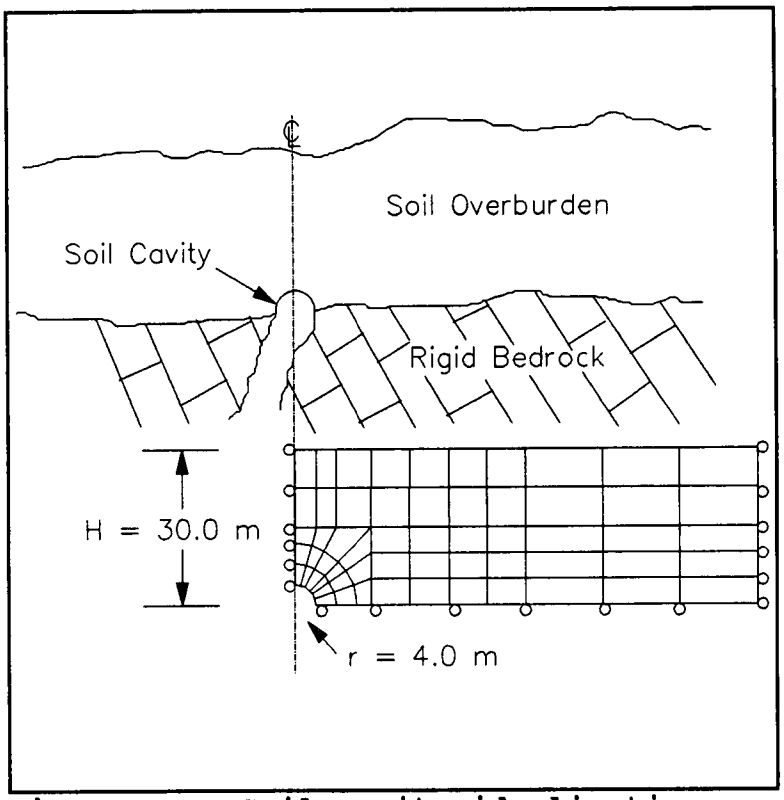


Figure 4.4 Soil-cavity idealization

gravitational forces while hydraulic forces were neglected. The soil cavity radii considered were 0.3, 0.6, 1.0, 2.0, and 4.0 meters. The thickness of overburden considered was 15.0, 22.5, 30.0, 37.5, and 45.0 meters. These values of cavity radius and depth of overburden cover the range found at East Chestnut Ridge.

Analysis of the results from the hyperbolic finite element model series identified two significant relationships: (1) the maximum vertical displacement is partially controlled by the radius of the soil cavity as shown in Figure 4.5, and (2) there is a linear relationship between basin half-width and the depth of overburden, Figure 4.6.

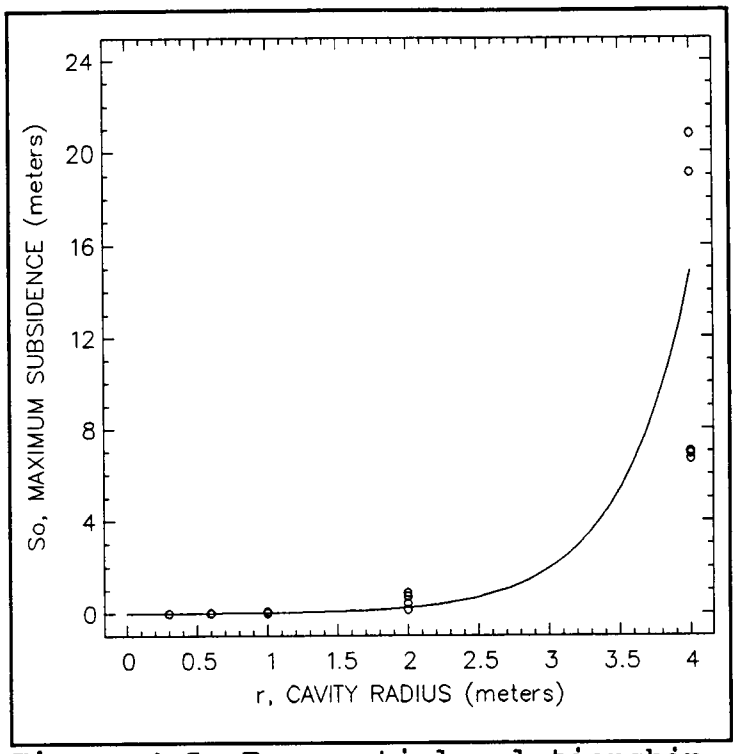


Figure 4.5 Exponential relationship between cavity radius and maximum subsidence from the numerical analysis

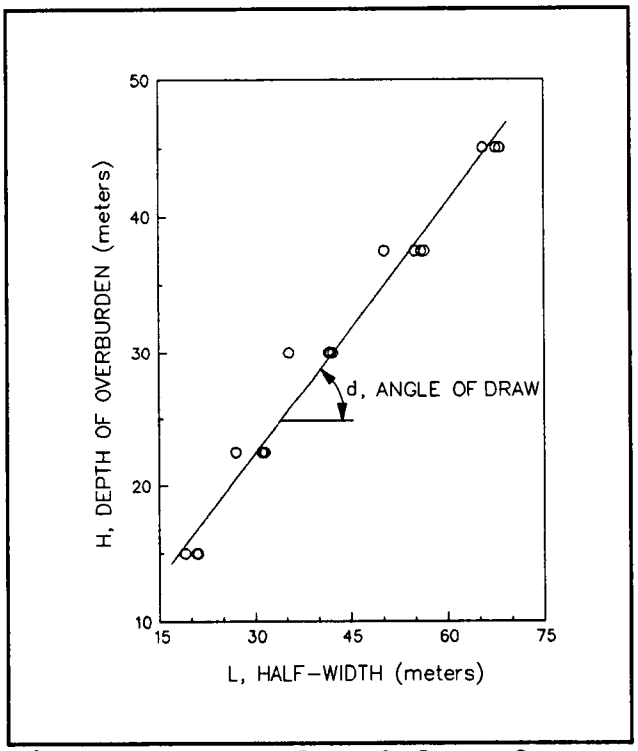


Figure 4.6 Angle of draw from the numerical analysis

An expression for the relationship between cavity radius and subsidence was found from regression to be exponential, with $R^2 = 0.933$. Maximum vertical displacement expressed in terms of cavity radius is:

$$S_0 = e^{-5.46 + 2.04\ r} \qquad [4.5]$$

where S_0 = the maximum vertical displacement, and r = the radius of the soil cavity, both in meters. An examination of the curve in Figure 4.5 shows that for a soil cavity radius less than 2 m there is little variation in maximum vertical displacement, and for large cavity radii, r = 4 m, there is significant scatter. The average observed maximum vertical displacement was approximately 2 m. This would require a soil cavity diameter of slightly more than 6 m.

The angle of draw was constant, $\delta = 31.9°$, as determined by linear regression, $R^2 = 0.980$, on the results of the numerical analysis. This is in contrast to the angle of draw, $\delta = 56.3°$ from field observations.

An additional analysis with r = 8.0 m and H = 45.0 m provided a value for the angle of draw, $\delta = 47.3°$. However, the cavity-soil idealization did not produce convergent results beyond 40% of the maximum loading. This suggests extreme vertical displacement of the soil directly above the soil cavity, and the formation a cover-collapse feature at the surface.

A relationship similar to that expressed in Equation 4.2 existed in the finite element profiles, between the distance to the inflection point and the half-width. This relationship, $R^2 = 0.923$, is also linear, and can be represented by the expression:

$$B = 0.49\ L - 0.29 \qquad [4.6]$$

where B = the distance to the inflection point and L = the half-width of the subsidence basin, both in meters. Figure 4.7 shows this relationship. Again, the intercept is small relative to the variable and can be neglected. The value of

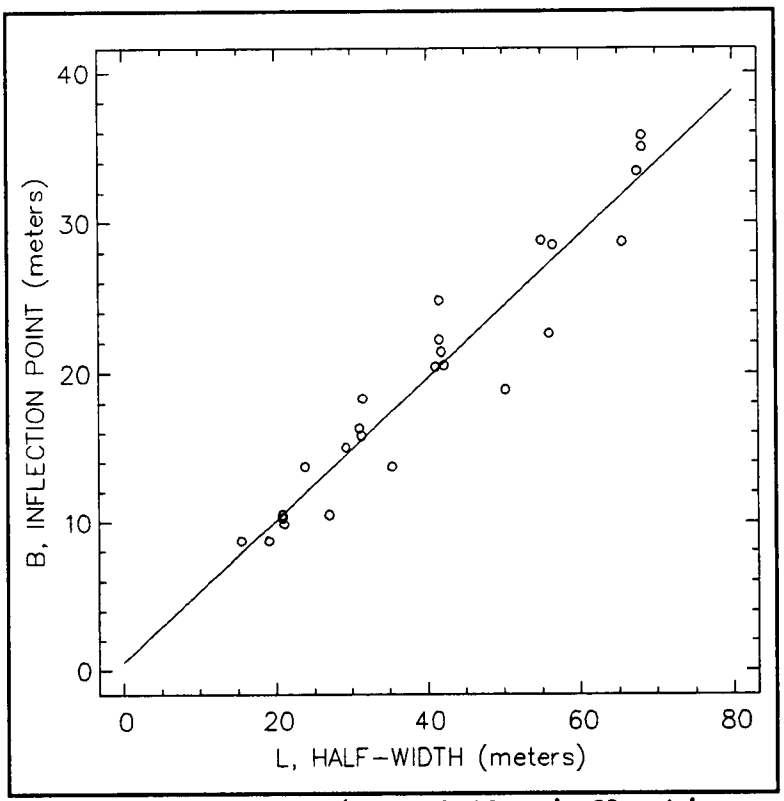


Figure 4.7 Location of the inflection point relative to basin half-width from the numerical analysis

0.49 suggests that the profiles can be generally described as not having a flat-bottom, with the maximum subsidence occurring only at a single point. This relationship between L and B provides the means for locating the inflection point in a predictive model. For the 25 hyperbolic finite element analyses the empirical parameters β and C maintained a linear relationship to each other. Geometric and empirical parameters defining the fit of both profile functions to the numerical subsidence basins is presented in Appendix B.

The basins resulting from the series of numerical analysis provided:

1) Magnitudes of vertical displacement that bracketed observed field values for large values of the soil cavity radii, r > 2 m

2) Half-widths consistently larger than observed values

3) Profiles without the characteristic flat-bottomed shape found in the field.

The last two suggest, that if insitu gravitational forces are the primary driving force of surface deformation, then either:

1) The hyperbolic, elastic, material model does not accurately replicate field behavior, or

2) The model parameters chosen do not replicate field conditions, or

3) Alternatively, hydraulic forces may be more significant than suggested by Chen and Beck (1989).

4.3 Site Subsidence Prediction

Direct substitution of Equation 4.5, maximum subsidence from soil cavity radius, into the predictive exponential function, Equation 4.3, yields an expression for the vertical displacement at any point. This expression is:

$$S(x) = e^{-5.46 + 2.04\, r\left[e^{-2.5\left[\frac{X}{0.67\, H}\right]^{3.3}}\right]} \qquad [4.7]$$

where r and H define geometry. The units of all variables is meters.

A similar expression can be derived for the hyperbolic function using Equation 4.4. The predictive profile function is:

$$S(x) = 0.5\, e^{-5.46 + 2.04\, r\left[1 - \tanh \frac{2.37\, X}{H}\right]} \qquad [4.8]$$

where the variables are as defined above.

4.4 Induced Ground Movements

The damage-causing parameters of angular distortion, deflection ratio, and radius of curvature can be directly calculated from a profile function describing the subsidence basin. Table 4.1 presents, in bold, the critical damage values from Table 2.2 for functional damage to masonry structures for constant basin half-width, L = 20.0 m, with increasing values of maximum vertical displacement. Values

are calculated from the exponential function. The observation length for calculation of angular distortion and deflection ratio is 4 m. Radius of curvature is calculated at a single point. All three damage parameters are calculated about the points of maximum slope or curvature of the profile.

The table indicates that very little vertical displacement is required to reach the critical damage limits suggested by Bhattacharya et al. (1984). It is important to note that the calculated deformations are for the ground surface. These movements must be transferred to the structure for damage to occur. Structural deformations tend to be less than those of the ground.

Table 4.2 is a back calculation of the required soil cavity radius, from Equation 4.5, for the critical values of maximum subsidence found in Table 4.1.

Table 4.1 Critical values for structural damage from sinkhole subsidence at East Chestnut Ridge.

Maximum Subsidence (meters)	Angular Distortion ($x10^{-3}$)	Deflection Ratio ($x10^{-3}$)	Radius of Curvature (km)
S_0 = 0.005	0.4	<0.1	**20.0**
S_0 = 0.03	**2.5**	0.2	3.16
S_0 = 0.09	7.5	**0.5**	1.05
S_0 = 2.0	163.5	10.2	0.05

S_0 = 2 m, average field value
L = 20.0 meters, constant

Critical values are in **bold.**

Table 4.2 Required soil cavity radius for values of critical maximum subsidence

S_o (meters)	r (meters)
0.005	0.08
0.03	0.96
0.09	1.50
2.0	3.02

The magnitudes of the vertical subsidence measured at the site are much greater than the critical values, shown above. This suggests catastrophic damage, for masonry structures, if sinkhole formation and surface structure are collocated. Extrapolation for landfill liner systems, suggests resistance to such deformation would require a structure of sufficient areal extent and strength to bridge the subsidence basin. The design of any structure where sinkhole subsidence is likely to occur would require an increased safety factor, due to the uncertainty about subsidence location and uncertainty about the magnitude of maximum vertical displacement.

CHAPTER 5 CONCLUSIONS

5.1 Conclusions

The sinkhole subsidence basins mapped at the site could be accurately described using profile functions. The negative exponential function generally provided a better fit to field and finite element profiles, and was easier to work with, than the hyperbolic tangent function.

The lateral extent of sinkhole subsidence is linearly related to the depth of overburden, as indicated by field measurements of basin width and borings to rock, and numerical analysis of the deformation of a cavity-residual soil system. Field observations suggest that this relationship can be expressed as an angle of draw which defines the lateral extent of subsidence from soil properties, or rather correlates with the case of active earth pressure.

The magnitude of vertical displacement cannot be predicted without idealization of the subsurface. Numerical analysis suggests a limited exponential relationship between the radius of a soil cavity and maximum vertical displacement. It is likely that actual soil cavity radii are less than 4 m in diameter. For small cavity radii, the formation of an arch in the soil around the cavity may limit the vertical displacements. The vertical gradient associated with the flow of an unconfined aquifer into

discontinuities in the bedrock may be the driving force which flattens the bottoms of the field subsidence basins. Hydraulic forces were neglected in the finite element analyses.

Observed values of subsidence are much greater than that required to cause severe damage to masonry surface structures. Uncertainty about the behavior of earth structures above a subsidence event indicate that conservative design is prudent.

5.2 Recommendations for Future Work

The solution of subsidence related earth-structure interaction problems has been approached in three parts. Movements of the ground surface could be more accurately predicted if the subsurface mechanical behavior of sinkholes was better understood. This includes the formation, extent, and erosion of an arch in the soil over a bedrock cavity; and a ratio of effect between gravitational and hydraulic forces. The interface between soil and structure, and the behavior of earth structures and demi-earth structures such as geotextiles and geomembranes, under physical and hydraulic loads will continue to be of geomechanical interest.

REFERENCES

REFERENCES

Beck, B.F., (1984). "Sinkhole Terminology," Proceedings, 1st Multidisciplinary Conference on Sinkholes, Orlando, Florida, pg. ix-x.

Ben-Hassine, J., (1987). "Finite Element Applications in the Analysis of Nonlinear Problems in Geomechanics," M.E. Thesis, University of Tennessee, Knoxville.

Bhattacharya, S., Singh, M.M., and Chen C.Y., (1984). "Proposed Criteria for Subsidence Damage to Buildings," Proceedings, 25th U.S. Symposium on Rock Mechanics, Northwestern University, Evanston, Illinois, pg 747-755.

Brauner, G., (1973). "Subsidence Due to Underground Mining (in two parts)," Information Circular 8571, U.S. Bureau of Mines.

Chen, D. and Peng, S.S., (1981). "Analysis of Surface Subsidence Parameters due to Underground Longwall Mining in the Northern Appalachian Coalfield," Technical Report 81-1, Department of Mining Engineering, West Virginia University.

Chen, J. and Beck, B.F., (1989). "Qualitative Modeling of the Cover-Collapse Process," Proceedings, 3rd Multidisciplinary Conference on Sinkholes, St. Petersburg, Florida, pg. 89-95.

Drumm, E.C., Bennett, W.F., Kane, W.F., (1988). "Mechanisms of Subsidence Induced Damage and Techniques for Analysis," ASCE Geotechnical Special Publication #19, pg 168-188.

Drumm, E.C., Kane, W.F., Ketelle, R.H., Ben-Hassine, J., and Scarborough, J.A., (1989), "Strength and Deformation Characteristics of Residual Soils Over Cavitose Bedrock," Oak Ridge National Laboratory, under Contract #R01133275, in preparation.

Duncan, J.M. and Chang, C.Y., (1970). "Nonlinear Analysis of Stress and Strain in Soils," Journal of Soil Mechanics, Foundation Division, ASCE, 96(SM5), pg. 1629-1653.

Geologic Associates Division, ERC/EDGe, (1989). "East Chestnut Ridge Soil Investigation, Oak Ridge, Tennessee," File #B435, Unpublished.

Illinois Mine Subsidence Insurance Fund, (1987). "The Illinois Mine Subsidence Insurance Fund Annual Report, 1986", Chicago, Illinois.

Karmis, M., editor, (1987). "Prediction of Ground Movements due to Underground Mining in the Eastern United States Coalfield, Vol. 1: Development of Prediction Techniques," Department of Mining and Minerals Engineering, Virginia Polytechnical Institute and State University.

Kemmerly, P.R., (1980). "Sinkhole Collapse in Montgomery County, Tennessee," Tennessee Division of Geology, Environmental Geology Series #6.

Kettelle, R.H. and Huff D.D., (1984). "Site Characterization of the West Chestnut Ridge Site," ORNL/TM-9229, Oak Ridge National Laboratory.

Kulhawy, F.H., (1983). "Transmission Line Structure Foundations for Uplift-Compression Loading," Electric Power Research Institute.

Myers, J.W., (1982). "Engineering Properties of the Soils of the Knox Group," Unpublished paper.

National Coal Board, (1975). "Subsidence Engineers Handbook," NCB Mining Department, United Kingdom.

Newton, J.G., (1976). "Early Detection and Correction of Sinkhole Problems in Alabama, with a Preliminary Evaluation of Remote Sensing Applications," Alabama Highway Department.

Newton, J.G., (1984). "Review of Induced Sinkhole Development," Proceedings, 1st Multidisciplinary Conference on Sinkholes, Orlando, Florida, pg. 3-9.

Peng, S.S. and Chaing, H.S., (1984). "Longwall mining," John Wiley and Sons.

STSC, (1988). "STATGRAPHICS, Statistical Graphics System User's Guide, University Edition," Statistical Graphics Corporation, 2115 East Jefferson Street, Rockville, Maryland.

Suits, L.D., Carroll, Jr., and Christopher, B.R., (1987). "ASTM Geotextile Committee Testing Update," ASTM Special Technical Publication #952, ASTM, pg. 161-175.

Tensar, (1986). "Tensar Drainage Nets for Leachate Collection at Waste Containment Facilities," Tensar Technical Note: WM1, Tensar Corporation, 1210 Citizens Parkway, Morrow, Georgia

Wilson, W.L. and Beck, B.F., (1988). "Evaluating Sinkhole Hazards in Karst Terrane," Geotechnical Special Publication #14, ASCE, pg. 1-24.

Whitman, R.V. and Bielak, J., (1980). "Foundations," in Chapter 7 of Design of Earthquake Resistant Structures, John Wiley and Sons

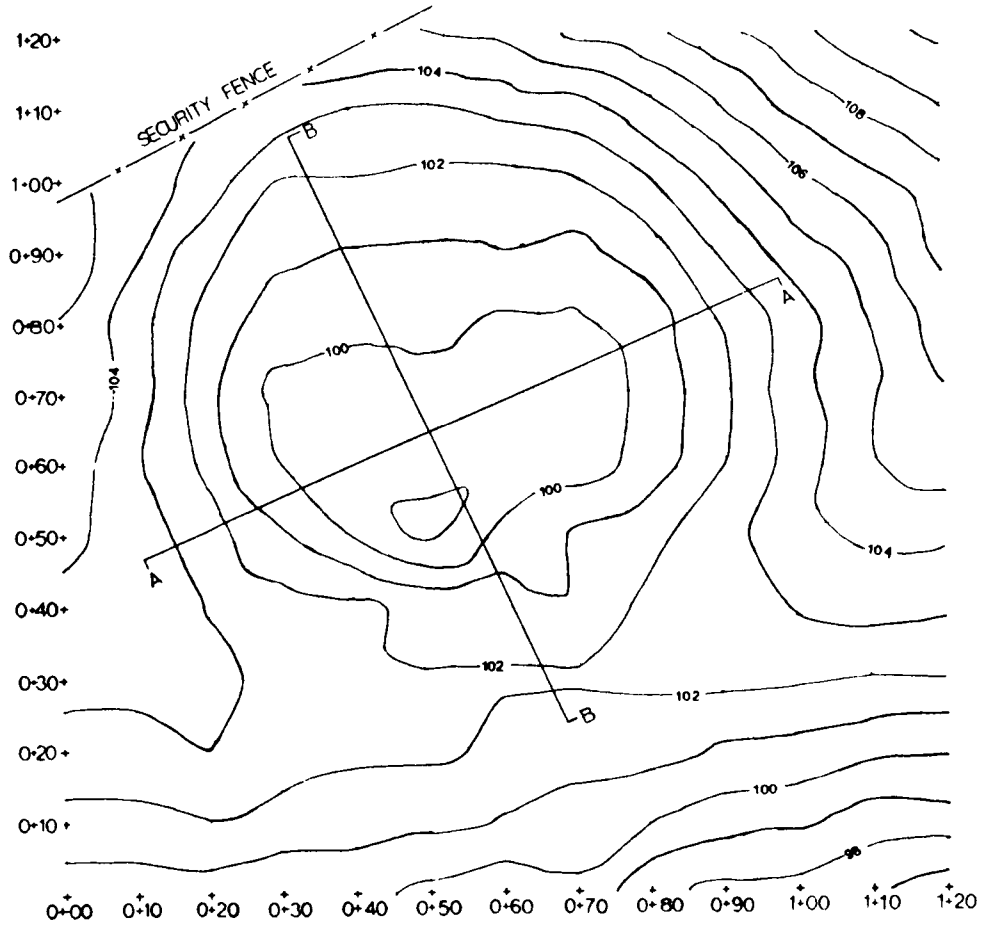
Woodward-Clyde Consultants, (1984). "Subsurface Characterization and Geohydrologic Evaluation, West Chestnut Ridge Site," ORNL/Sub/83-647/641/V1-2, in two volumes, Oak Ridge National Laboratory.

Yoon, C.J., (1987). "Slip Surfaces in Sinkholes: An Analysis of the Slip Line of an Axisymmetric Open Karst Pipe." M.S. Thesis, University of Tennessee, Knoxville.

APPENDIXES

APPENDIX A

SINKHOLE TOPOGRAPHIC MAPS



EAST CHESTNUT RIDGE SITE
SINKHOLE #01

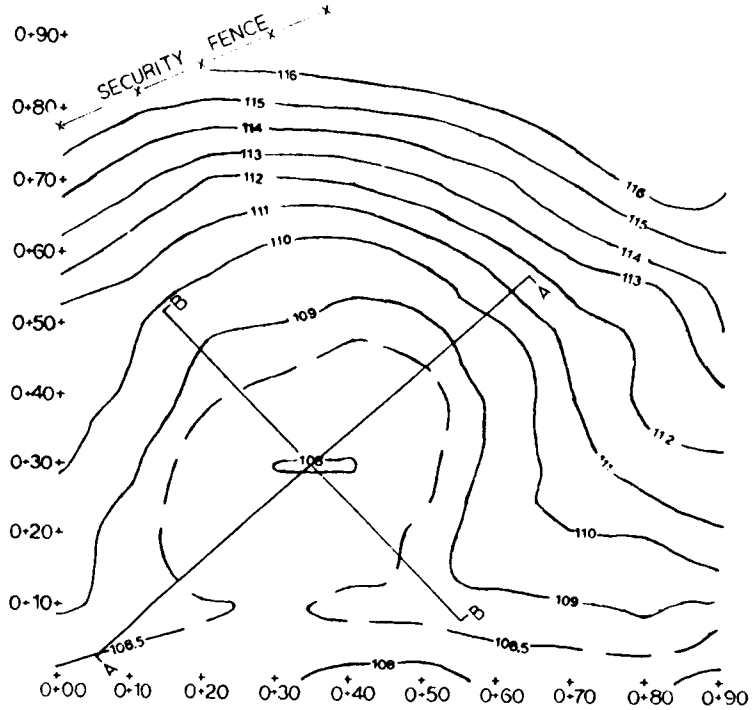
SITE LOCATION

10 0 5 10 20

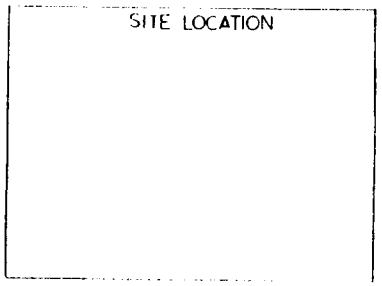
M N
W E
S

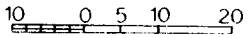
ELEVATIONS TO AN ARBITRARY DATUM

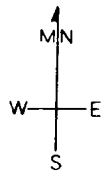
UNIVERSITY OF TENNESSEE	CONTOUR INTERVAL 1 FOOT			SEC.
SCALE: 1"=10'	DATE: 1/25/89	DRAWN BY: JESSEE SCARBOROUGH	CK BY:	NO. 01



EAST CHESTNUT RIDGE SITE
SINKHOLE #02

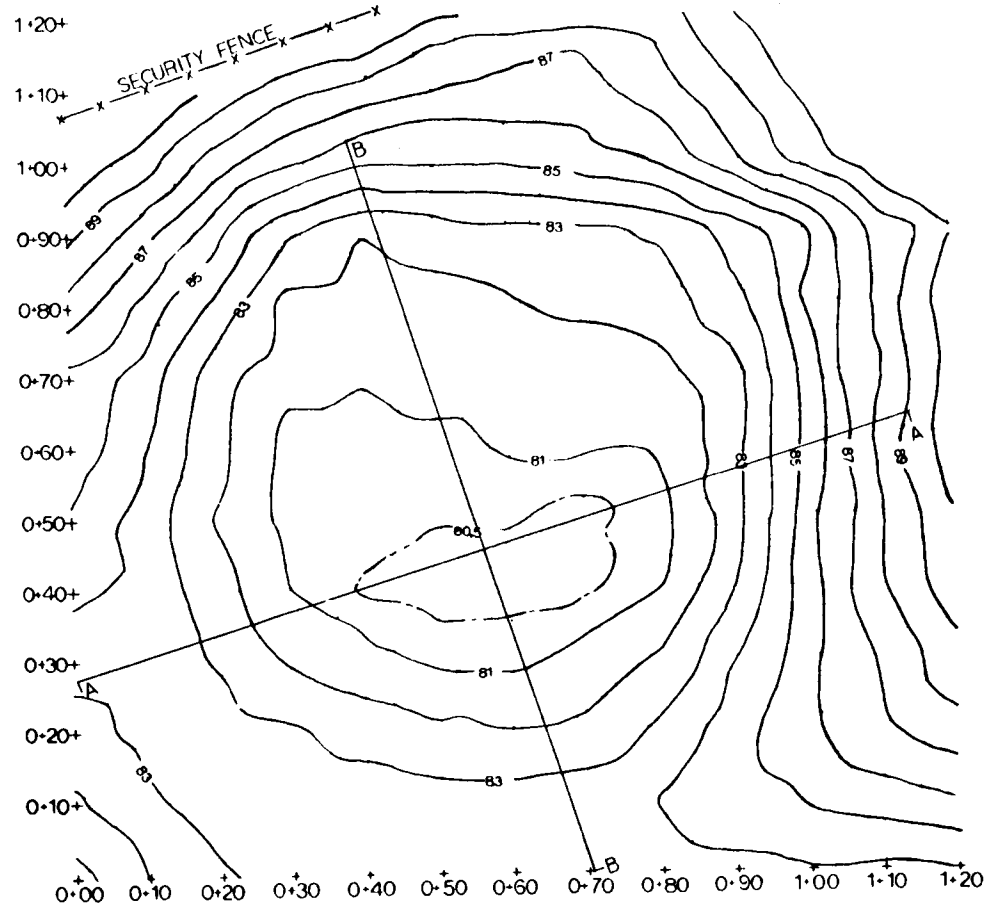






ELEVATIONS TO AN ARBITRARY DATUM

UNIVERSITY OF TENNESSEE	CONTOUR INTERVAL 1 FOOT		SEC.
SCALE: 1"=10'	DATE: 2/02/89	DRAWN BY: JESSEE SCARBOROUGH	CK BY:	NO. 02



EAST CHESTNUT RIDGE SITE
SINKHOLE # 03

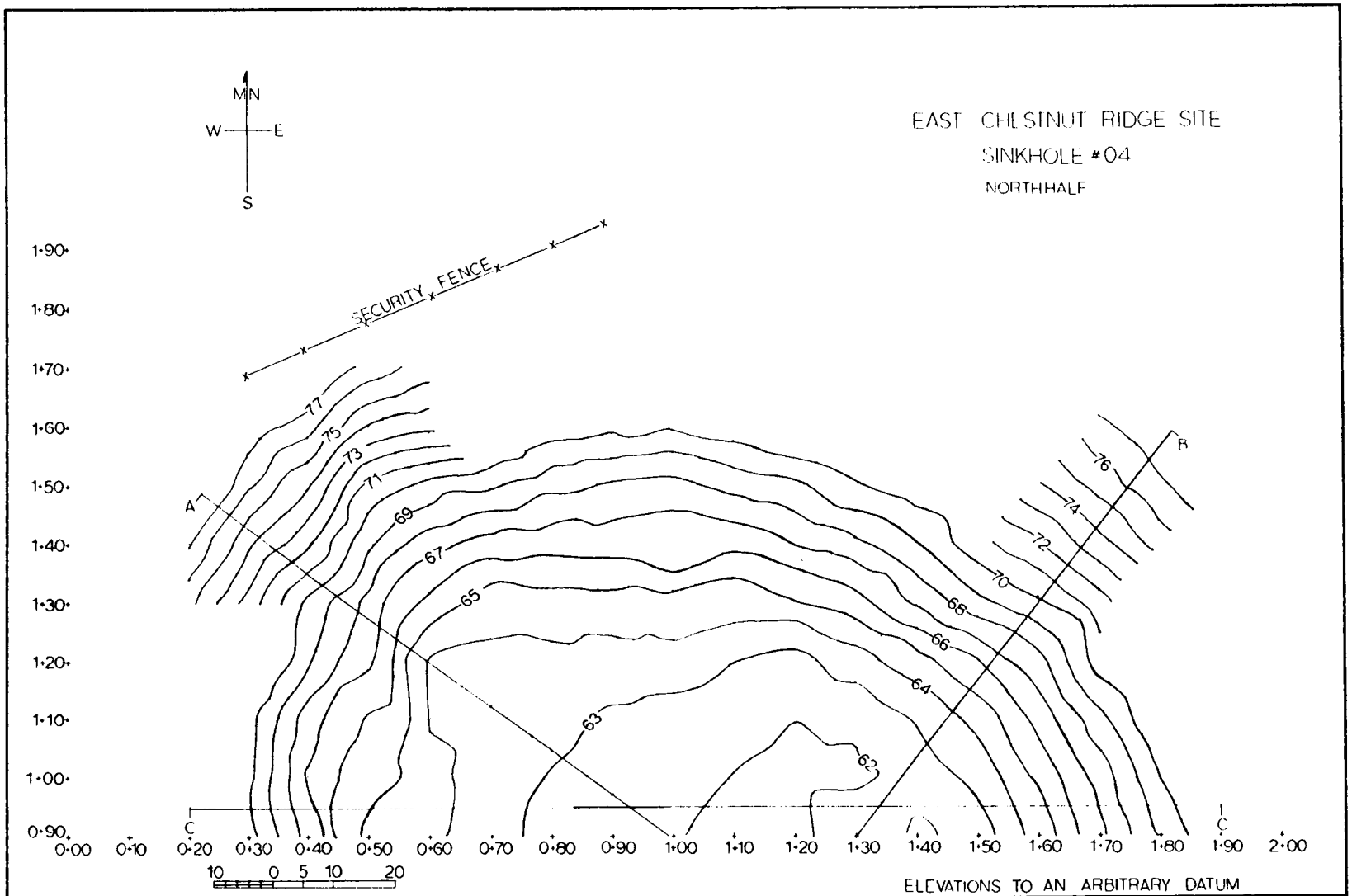
SITE LOCATION

10 0 5 10 20

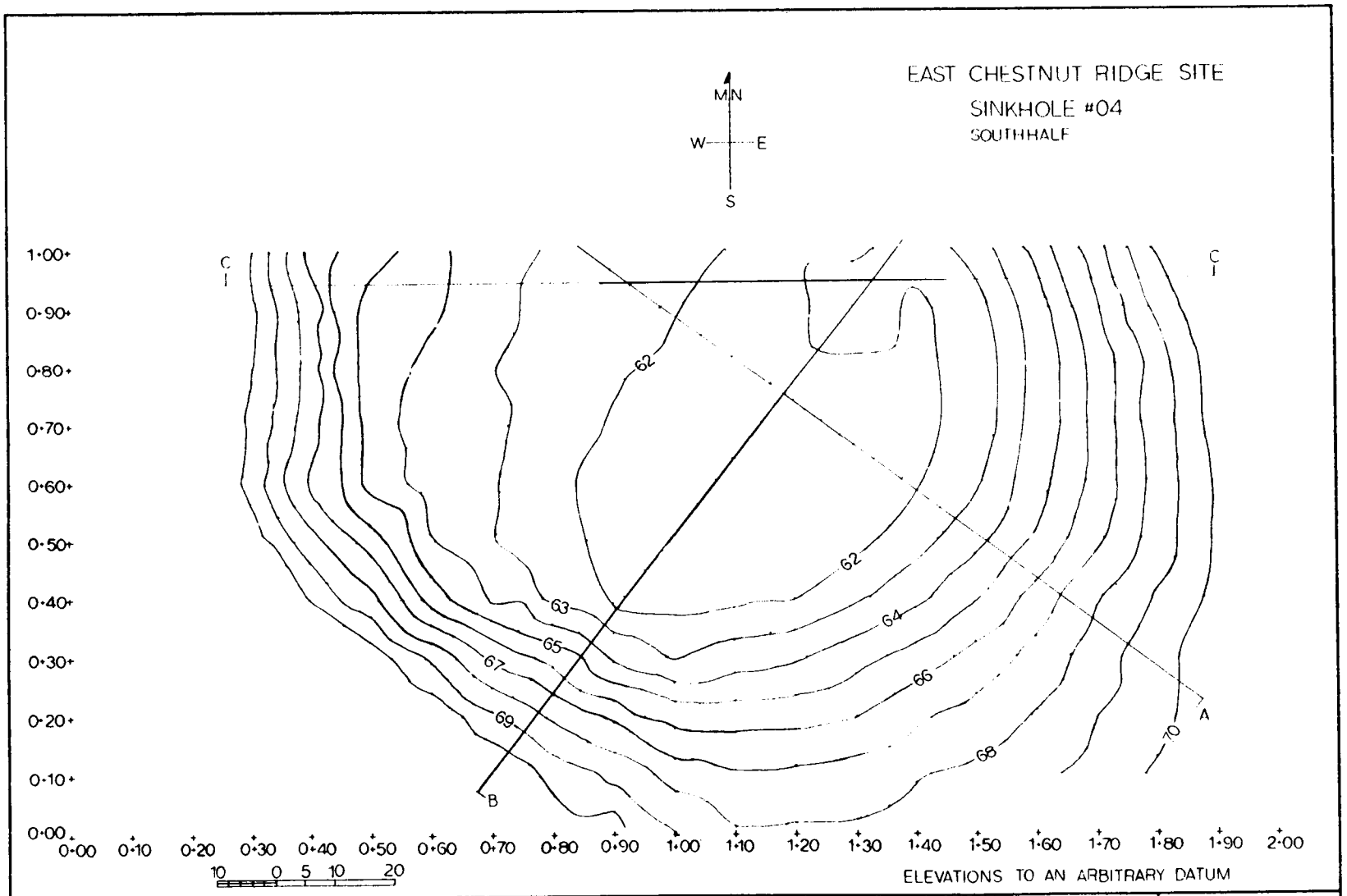
MN
W E
S

ELEVATIONS TO AN ARBITRARY DATUM

UNIVERSITY OF TENNESSEE	CONTOUR INTERVAL 1 FOOT	SEC.
SCALE: 1"=10'	DATE: 3/15/89	DRAWN BY: JESSEE SCARBOROUGH	CK BY:	NO. 03

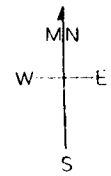


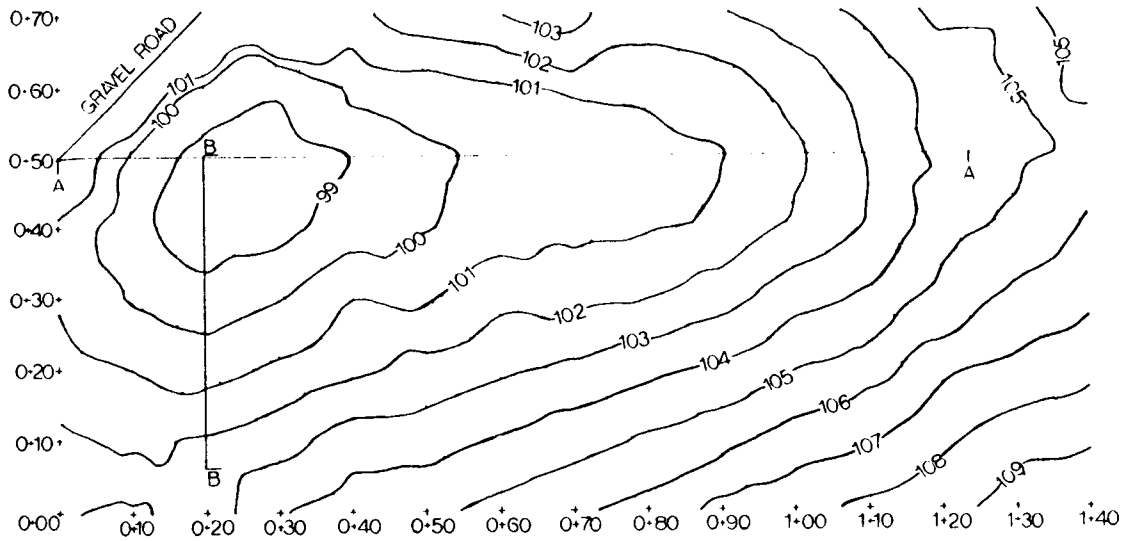
UNIVERSITY OF TENNESSEE	CONTOUR INTERVAL 1 FOOT			**SEC.**
SCALE: 1 INCH = 10 FEET	**DATE:** 5/28/89	**DRAWN BY:** JESSEE SCARBOROUGH	**CK BY:**	**NO.** 04 NORTH



UNIVERSITY OF TENNESSEE	CONTOUR INTERVAL 1 FOOT			SEC.
SCALE: 1 INCH = 10 FEET	DATE: 5/23/89	DRAWN BY: JESSEE SCARBOROUGH	CK BY:	NO. 04 south

EAST CHESTNUT RIDGE SITE
SINKHOLE #06

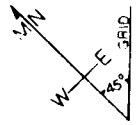




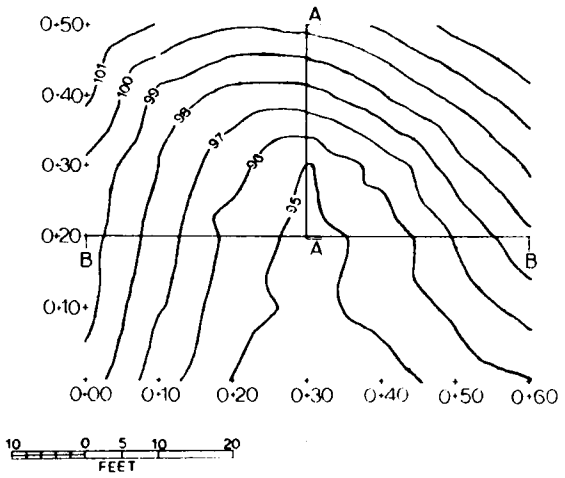
10 0 5 10 20
FEET

ELEVATIONS TO AN ARBITRARY DATUM

UNIVERSITY OF TENNESSEE	CONTOUR INTERVAL 1 FOOT			**SEC.**
SCALE: 1 INCH = 10 FEET	**DATE:** 6/1/89	**DRAWN BY:** JESSEE SCARBOROUGH	**CK BY:**	**NO.** 06



EAST CHESTNUT RIDGE SITE
SINKHOLE #07
"SADDLE

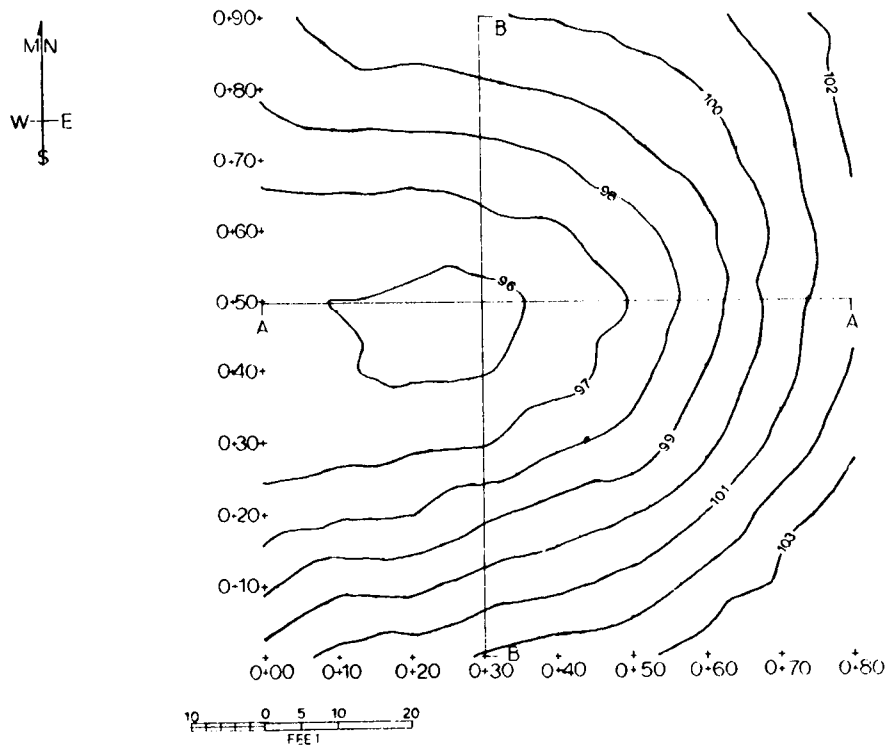


ELEVATIONS TO AN ARBITRARY DATUM

UNIVERSITY OF TENNESSEE	CONTOUR INTERVAL 1 FOOT		SEC.
SCALE: 1 INCH = 10 FEET	DATE: 7/13/89	DRAWN BY: JESSEE SCARBOROUGH	CK BY:	NO. 07

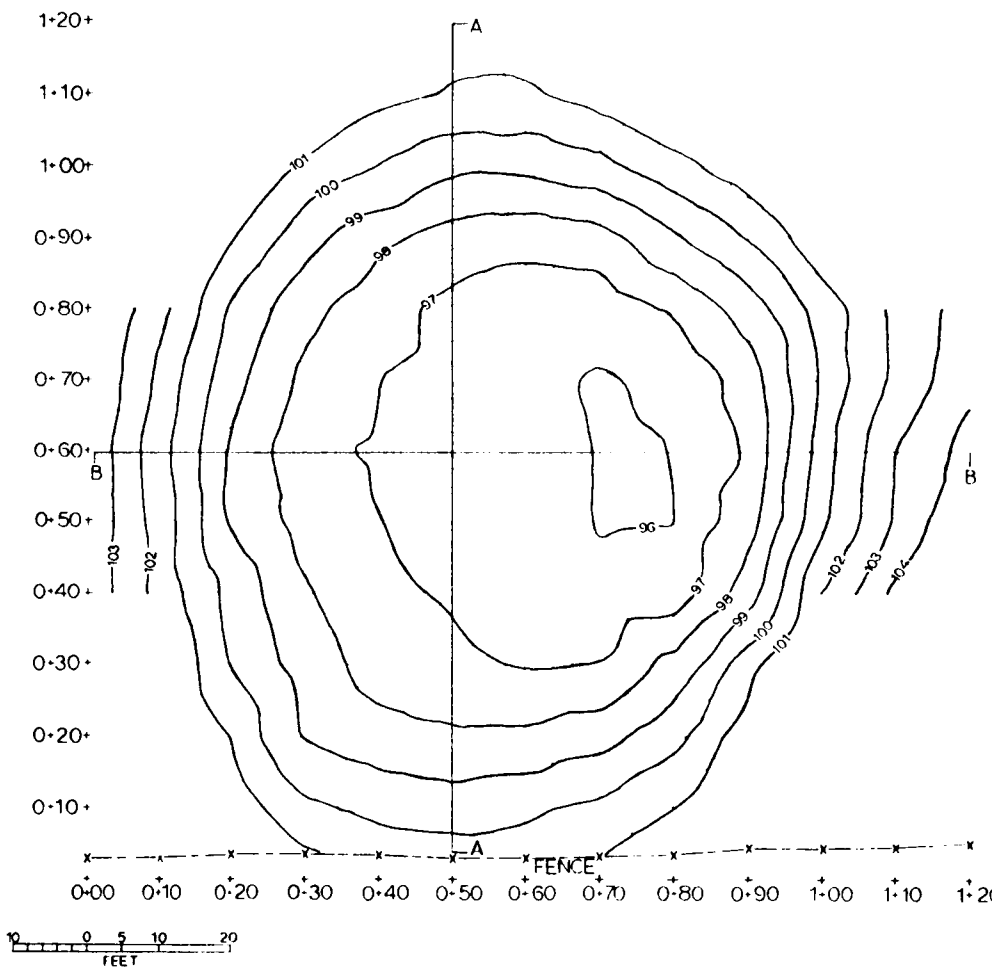
EAST CHESTNUT RIDGE SITE

SINKHOLE # 08



ELEVATIONS TO AN ARBITRARY DATUM

UNIVERSITY OF TENNESSEE	CONTOUR INTERVAL 1 FOOT		SEC.
SCALE: 1 INCH = 10 FEET	DATE: 7/17/89	DRAWN BY: JESSEE SCARBOROUGH	CK BY:	NO. 08

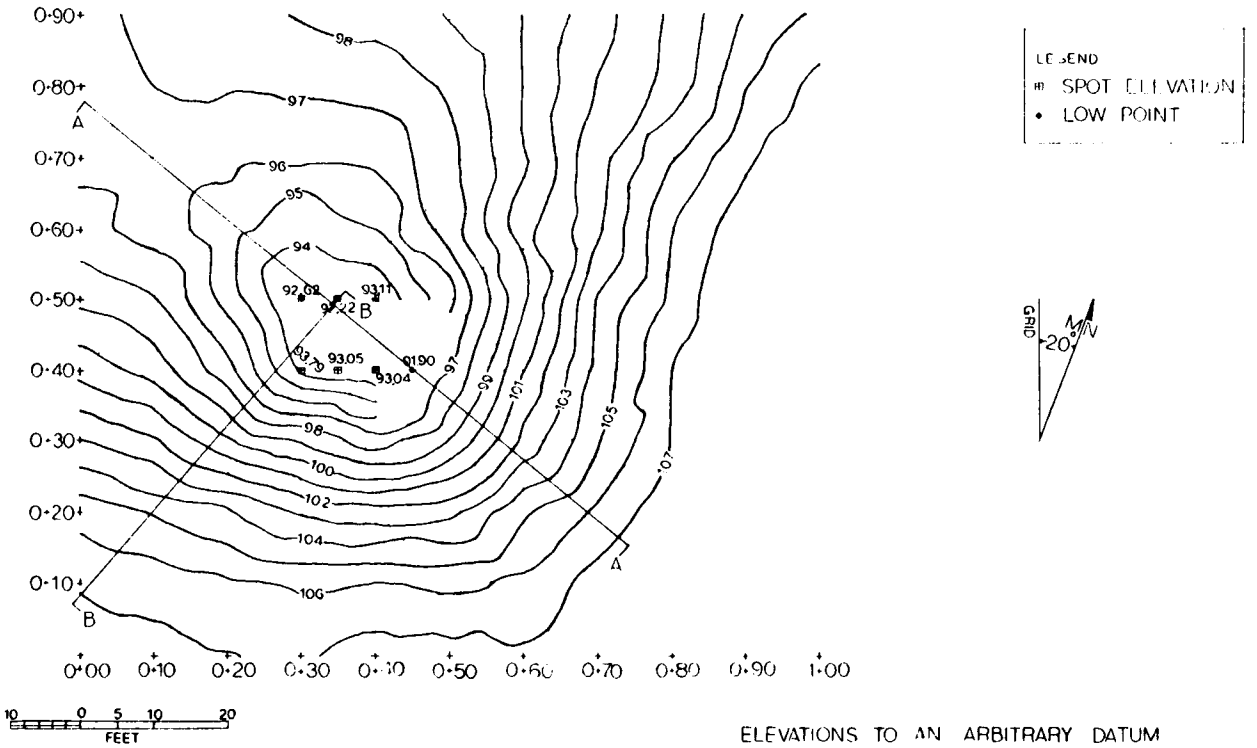


ELEVATIONS TO AN ARBITRARY DATUM

UNIVERSITY OF TENNESSEE	CONTOUR INTERVAL 1 FOOT		SEC.
SCALE: 1 INCH = 10 FEET	DATE: 7/23/89	DRAWN BY: JESSEE SCARBOROUGH	CK BY:	NO. 09

EAST CHESTNUT RIDGE SITE

SINKHOLE #11



ELEVATIONS TO AN ARBITRARY DATUM

UNIVERSITY OF TENNESSEE	CONTOUR INTERVAL 1 FOOT		SEC.
SCALE: 1 INCH = 10 FEET	DATE: 7/26/89	DRAWN BY: JESSEE SCARBOROUGH	CK BY:	NO. 11

APPENDIX B

EMPIRICAL AND GEOMETRIC PARAMETERS

B.1 Field Profiles and the Exponential Function

Profile	S_0 (m)	L (m)	α	β	R^2
01 west	1.28	15.2	4.35	4.44	0.997
01 east	1.31	15.2	3.78	4.82	0.996
01 south	0.88	10.7	4.38	3.24	0.974
01 north	1.04	15.2	2.93	2.59	0.973
02 west	0.23	9.1	2.65	3.82	0.957
02 east	2.44	18.3	3.06	3.87	0.996
02 south	0.20	6.7	3.15	3.11	0.997
02 north	1.53	15.2	2.96	3.31	0.978
03 west	0.94	15.2	4.16	4.11	0.998
03 east	2.61	18.3	2.76	4.27	0.994
03 south	0.96	12.2	3.65	3.40	0.994
03 north	2.59	21.3	2.44	5.47	0.987
04 west	4.68	30.5	3.15	3.69	0.995
04 east	2.57	22.9	3.01	6.64	0.994
04 south	2.57	24.4	3.30	3.53	0.999
04 north	4.69	36.6	2.76	5.21	0.983
06 east	2.08	34.23	2.07	2.32	0.942
06 south	1.22	13.08	2.95	3.33	0.995
06 west	1.17	5.85	-	-	-
07 north	1.74	8.81	3.44	4.15	0.999
07 east	1.26	8.75	2.78	2.82	0.995
07 west	1.49	8.81	2.53	2.46	0.988
08 west	0.30	8.53	2.69	1.33	0.992
08 east	1.87	14.51	2.54	2.79	0.987
08 north	1.31	11.61	2.21	1.78	0.971
08 south	1.96	14.63	2.62	2.92	0.995
09 north	1.45	16.58	3.46	4.69	0.999
09 south	1.20	16.98	2.39	4.47	0.989
09 east	2.58	20.45	3.77	5.78	0.990
09 west	2.21	14.81	2.56	4.02	0.991
10 south	5.40	63.79	2.40	4.11	0.968
10 north	1.67	23.53	2.35	3.08	0.991
10 north/east	2.55	35.30	2.50	2.74	0.996
10 north/west	1.12	29.32	1.99	2.37	0.956
10 south/east	2.26	23.16	2.54	2.31	0.993
10 south/west	5.14	46.24	2.52	3.51	0.997

Profile	S_0 (m)	L (m)	α	β	R^2
11 north	1.23	9.75	2.85	1.87	0.995
11 south	4.60	14.26	2.97	2.45	0.972
11 west	4.50	14.48	2.84	1.91	0.999
Average all profiles:			2.93	3.49	
Composite best fit:			2.50	3.30	0.926

B.2 Field Profiles and the Hyperbolic Function

Profile	S_0 (m)	B (m)	C	R^2
01 west	1.28	10.00	3.36	0.996
01 east	1.31	10.85	3.67	0.990
01 south	0.88	6.37	2.42	0.970
01 north	1.04	9.54	2.07	0.961
02 west	0.23	6.49	2.65	0.956
02 east	2.44	12.53	2.84	0.994
02 south	0.20	4.15	2.32	0.995
02 north	1.53	10.24	2.54	0.975
03 west	0.94	10.03	3.10	0.995
03 east	2.61	13.47	3.21	0.987
03 south	0.96	7.77	2.67	0.990
03 north	2.59	16.98	3.99	0.983
04 west	4.68	20.30	2.69	0.995
04 east	2.57	18.23	4.83	0.993
04 south	2.57	15.73	2.65	0.997
04 north	4.69	28.41	3.78	0.978
06 east	2.08	24.38	1.90	0.914
06 south	1.22	8.96	2.63	0.985
06 west	1.17	3.78	2.30	0.989
07 north	1.74	5.97	3.28	0.998
07 east	1.26	5.36	2.09	0.994
07 west	1.49	5.33	1.86	0.987
08 west	0.30	3.05	1.05	0.956
08 east	1.87	9.51	2.12	0.986
08 north	1.31	6.68	1.44	0.971
08 south	1.96	9.24	2.16	0.993
09 north	1.45	11.80	3.50	0.998
09 south	1.20	13.11	3.34	0.983
09 east	2.58	14.94	4.37	0.990
09 west	2.21	10.82	2.94	0.988

Profile	S_0 (m)	B (m)	C	R^2
10 south	5.40	48.49	2.92	0.964
10 north	1.67	16.34	2.32	0.987
10 north/east	2.55	21.70	2.00	0.992
10 north/west	1.12	18.99	1.69	0.971
10 south/east	2.26	13.53	1.74	0.995
10 south/west	5.14	32.10	2.59	0.996
11 north	1.23	4.48	1.46	0.981
11 south	4.60	7.35	1.70	0.952
11 west	4.50	6.92	1.40	0.993
Average all profiles:			2.60	
Composite best fit:			2.63	0.967

B.3 Numerical Profiles, Geometric Parameters

Profile (m)	r/H	S_0 (m)	L (m)	B (m)
r = 0.3, H = 15.0	0.0200	0.001	20.85	10.5
= 22.5	0.0130	0.003	31.08	16.3
= 30.0	0.0100	0.005	41.57	22.2
= 37.5	0.0080	0.007	54.98	28.8
= 45.0	0.0067	0.008	68.14	35.8
r = 0.6, H = 15.0	0.0400	0.006	20.90	10.3
= 22.5	0.0267	0.012	31.35	15.8
= 30.0	0.0200	0.019	41.86	21.4
= 37.5	0.0160	0.020	56.49	28.5
= 45.0	0.0133	0.031	68.20	35.0
r = 1.0, H = 15.0	0.0667	0.019	21.08	9.9
= 22.5	0.0444	0.036	31.52	18.3
= 30.0	0.0333	0.058	42.21	20.5
= 37.5	0.0267	0.084	55.99	22.6
= 45.0	0.0222	0.076	67.55	33.4
r = 2.0, H = 15.0	0.1333	0.158	19.08	8.7
= 22.5	0.0889	0.432	26.99	10.5
= 30.0	0.0667	0.882	35.34	13.7
= 37.5	0.0533	0.721	50.25	18.9
= 45.0	0.0444	0.429	65.55	28.7
r = 4.0, H = 15.0	0.2667	6.904	15.46	8.7
= 22.5	0.1778	6.677	23.83	13.7
= 30.0	0.1333	7.001	29.25	15.0
= 37.5	0.1067	19.080	41.11	20.5
= 45.0	0.0889	20.760	41.59	24.8

B.4 Numerical Profiles, Exponential Function

Profile (m)	r/H	α	β	R^2
r = 0.3, H = 15.0	0.0200	2.82	2.10	0.992
= 22.5	0.0130	2.96	2.23	0.995
= 30.0	0.0100	2.91	2.28	0.999
= 37.5	0.0080	3.05	2.26	0.999
= 45.0	0.0067	3.02	2.29	0.999
r = 0.6, H = 15.0	0.0400	3.03	2.09	0.996
= 22.5	0.0267	3.01	2.15	0.997
= 30.0	0.0200	2.96	2.18	0.999
= 37.5	0.0160	3.10	2.23	0.999
= 45.0	0.0133	3.02	2.22	0.999
r = 1.0, H = 15.0	0.0667	3.16	2.01	0.998
= 22.5	0.0444	3.09	2.05	0.998
= 30.0	0.0333	3.06	2.07	0.999
= 37.5	0.0267	3.21	2.06	0.999
= 45.0	0.0222	3.06	2.18	0.999
r = 2.0, H = 15.0	0.1333	3.65	1.86	0.998
= 22.5	0.0889	4.88	2.17	0.995
= 30.0	0.0667	4.96	2.14	0.996
= 37.5	0.0533	4.25	2.06	0.995
= 45.0	0.0444	3.54	2.05	0.998
r = 4.0, H = 15.0	0.2667	4.92	3.51	0.998
= 22.5	0.1778	3.57	2.92	0.999
= 30.0	0.1333	2.45	1.68	0.994
= 37.5	0.1067	3.12	2.13	0.998
= 45.0	0.0889	2.71	2.50	0.991

B.5 Numerical Profiles, Hyperbolic Function

Profile (m)	r/H	C	R^2
r = 0.3, H = 15.0	0.0200	1.62	0.989
= 22.5	0.0130	1.75	0.994
= 30.0	0.0100	1.77	0.997
= 37.5	0.0080	1.79	0.997
= 45.0	0.0067	1.81	0.997
r = 0.6, H = 15.0	0.0400	1.64	0.993
= 22.5	0.0267	1.68	0.995
= 30.0	0.0200	1.70	0.996
= 37.5	0.0160	1.74	0.996
= 45.0	0.0133	1.77	0.996

Profile (m)	r/H	C	R^2
r = 1.0, H = 15.0	0.0667	1.59	0.995
= 22.5	0.0444	1.72	0.975
= 30.0	0.0333	1.63	0.995
= 37.5	0.0267	1.41	0.956
= 45.0	0.0222	1.70	0.995
r = 2.0, H = 15.0	0.1333	1.55	0.990
= 22.5	0.0889	1.79	0.990
= 30.0	0.0667	1.77	0.992
= 37.5	0.0533	1.63	0.977
= 45.0	0.0444	1.65	0.988
r = 4.0, H = 15.0	0.2667	2.65	0.999
= 22.5	0.1778	2.22	0.999
= 30.0	0.1333	1.38	0.991
= 37.5	0.1067	1.67	0.997
= 45.0	0.0889	1.88	0.994

VITA

Jessee Americus Scarborough was born in California in 1961. Despite this, he grew up in Norris, Tennessee, and graduated from Norris High School. As an undergraduate, he attended the University of Virginia, on a four year Army ROTC scholarship, and finally received a BS in Civil Engineering in December of 1984. In the U.S. Army, he completed Airborne training and was assigned as a Topographic Engineer. Three and one-half years later, he began study at The University of Tennessee in Knoxville toward a MS in Civil Engineering.

He intends to work for the Geotechnical Division of ERC/EDGe as a Staff Geotechnical Engineer.